Driving Japan's Green Transition: An Advanced Modeling Framework for Grid Stability and Renewable Integration

Ravikumar Shah*, Tanvi Bhatt, Jay Parmar, Mayur Barbhaya

[a] *Research and Development Department, VeBuIn, Japan*

Abstract

The increasing integration of photovoltaic (PV) systems into Japan's power grid presents significant challenges for grid stability and energy forecasting, primarily due to the intermittent nature of solar power. A key impediment to accurate power output prediction is the difficulty in precisely estimating PV cell parameters from the limited information available on manufacturer datasheets. This study proposes and validates a robust methodology to extract comprehensive PV parameters using advanced metaheuristic optimization for both single-diode and double-diode models. We apply and compare several algorithms, including Best–Worst–Random (BWR), Best-Mean-Random (BMR), and JAYA, utilizing data from three distinct module types: polycrystalline, monocrystalline, and thin-film. The optimization process minimizes the error between the model's calculated I-V characteristics and the empirical data at the open-circuit, short-circuit, and maximum power points. The results demonstrate that the proposed metaheuristic approach successfully identifies optimal parameter sets, achieving a precise match with experimental I-V and P-V curves. This enhanced modeling accuracy provides a reliable foundation for predicting energy production, facilitating more effective grid management and operational planning for Japanese power utilities and supporting the nation's transition to a renewable-centric power system.

Keywords: Best–Worst–Random (BWR) algorithm, Jaya algorithm, Best-Mean-Random (BMR), Parameter estimation, Single-diode model, Double-diode model, Metaheuristic optimization, Energy forecasting, Photovoltaic modeling

1. Introduction

Power generation business are shifting toward renewable energy sources, and substantial research is dedicated to improving their continuous performance Rashid (2024). japan's power utilities, like those globally, face challenges in maintaining the reliability and maximizing the return on investment of solar photovoltaic installations Hopwood and Gunda (2022). One critical aspect involves accurately modeling PV systems to predict energy production and optimize operational parameters Gayibov and Abdullaev (2021). The intermittent nature of solar energy and the complexities of real-world operating conditions make precise modeling essential for grid stability and economic viability Salazar-Peña et al. (2024). An accurate model is also required to predict the energy available from the array King et al. (2003).The fact that manufacturer datasheets usually only include open-circuit voltage, short-circuit current, and maximum power point characteristics is a major barrier. Ulapane et al. (2012). This necessitates robust parameter estimation techniques that can derive comprehensive PV characteristics from sparse data, enhancing power output prediction and facilitating optimal inverter design Muhsen et al. (2016) Mhanni and Lagmich (2024). To address these issues, enhanced methodologies are needed that improve traditional technologies in terms of accuracy and prediction precision for PV cell generation Kumar et al. (2024). The automated design of forecasting models is challenged by missing information regarding PV mounting configurations and the limited amount of historical data available for training, especially for new PV plants Meisenbacher et al. (2022). These models are crucial for optimizing the integration of solar energy into the grid and for predicting its performance under varying meteorological conditions Jiang et al. (2023). Accurate forecasting of PV power is crucial for the efficient integration of solar energy into power systems, enabling better planning, scheduling, and operation of the grid Leo et al. (2025). This is particularly important for grid-connected PV systems, those with integrated storage, and systems operating under dynamic demand-response schemes Leo et al. (2025).

Japan market faces unique challenges due to its high solar penetration and complex grid infrastructure, making accurate PV power forecasting and system modeling paramount for ensuring grid stability and optimizing energy resource use Kim et al. (2021) Lari et al. (2025). Accurate forecasting also helps reduce reserve capacity and prevent electrical energy system disruptions Assaf et al. (2023). Given the increasing integration of PV systems into power grids, precise PV output forecasts have become an efficient solution to manage variability and reduce operational costs Nguyen and Müsgens (2021). Therefore, the development of accurate and reliable PV power forecasting techniques is of great importance for maintaining grid stability and optimizing energy resource utilization Leo et al. (2025) Li

Email address: jay@vebuin.com (Jay Parmar), ravikumarshah@vebuin.com (* Corresponding author Ravikumar Shah), tanvibhatt@vebuin.com (Tanvi Bhatt), mayurbarbhaya@vebuin.com (Mayur Barbhaya)

et al. (2021). As solar energy becomes a more significant part of the electricity generation mix, the ability to accurately forecast the energy produced by PV systems becomes increasingly important Konstantinou et al. (2021). As demand for energy increases, integrating alternative energy sources like PV cell into the power grid becomes crucial for ensuring a reliable power supply Kumar et al. (2020) .

2. Background and Motivation

Achieving these objectives requires advanced machine learning algorithms and optimization techniques to manage the inherent unpredictability of PV generation (Soleymani and Mohammadzadeh, 2023). Significant work is now being done to develop real-time performance models that use a deployment's location and weather conditions to estimate solar output Chen and Irwin (2017). Japan's focus on strengthening the competitiveness and economic efficiency of thermal power generation, along with its initiatives to secure fuel and necessary installed capacity, highlights the need for accurate PV models to effectively integrate solar energy into the grid Yamazaki and Ikki (2022). Given that PV power generation is highly dependent on weather conditions, precise forecasting is difficult but necessary for stability, dependability, and scheduling of power system operations Iheanetu (2022). Accurate PV power forecasting necessitates identifying and predicting weather conditions impacting PV systems, often employing diverse data preprocessing techniques to enhance prediction capabilities Kohút and Kvasnica (2023) Carrera et al. (2020). To ensure long-term operation and maintenance of existing PV systems, predictive models play a crucial role in achieving the goal of introducing 120 GW of PV power generation by 2030 in Japan Yamazaki and Ikki (2022).

3. Literature Review

With the increasing adoption of renewable energy sources such as PV and wind power, the need for accurate power forecasting methods has become more critical for ensuring the safe and economic operation of power systems Liao et al. (2022). The need for precise PV power calculation for particular geographic areas is further highlighted by the erratic nature of solar energy and its reliance on meteorological factors like solar radiation and ambient temperature Chakraborty et al. (2023). By using statistical and machine learning techniques to anticipate PV production, these predictions can manage variability and lower operating costs related to solar power integration Kohút and Kvasnica (2023) Zhang et al. (2020). Integertion of PV in power producing companys requires the use of forecasting models to address reliability issues Riggs et al. (2023). Municipalities are progressively enhancing the deployment of renewable energy by establishing capacity goals, allocating specific promotion zones, installing photovoltaic systems in municipal buildings, and offering financial incentives, signaling a comprehensive move towards embracing solar energy. Yamazaki and Ikki (2022). These efforts are complemented by national projects aimed at decarbonization and accelerating the adoption of renewable energy sources, which include managing feed-in tariff schemes and promoting new development while reducing costs Yamazaki and Ikki (2022) . Business market of japan are also developing their solar sectors, especially in manufacturing photovoltaic cells and modules Yamazaki and Ikki (2022).

The goal is to create a stable supply-and-demand power grid systems by modeling solar photovoltaic generation prediction Kim et al. (2021).

Parameter estimation of solar cells using datasheet information with the application of an adaptive differential evolution algorithm" Biswas et al. (2018), details mathematical models for solar cells, specifically focusing on single-diode and double-diode models. The objective of the optimization in this study is to accurately estimate PV cell parameters to satisfy the current-voltage relationships at three major points: open circuit, short circuit, and maximum power points Biswas et al. (2018). Such an estimation is critical because experimental data or detailed characteristic data of a PV module may not always be readily available, making parameter estimation from datasheet values a practical necessity Biswas et al. (2018). For example, models could integrate machine learning techniques and data science tools to predict the power output of building-integrated photovoltaic systems across various building orientations, thereby enhancing the precision of PV power generation forecasts (Kabilan et al., 2021) (Maitanova et al., 2020) and ensemble techniques, like random forest and extreme gradient boosting, are well-suited for solar radiation prediction because they improve stability, reduce variation and bias, and combine several machine learning models (Mishra et al., 2023). Furthermore, improving the accuracy of hourly solar power forecasts can be achieved by including a PV-performance model as part of the data-mining stage (Pombo et al., 2022). This strategy makes it possible to integrate solar energy into current power systems in a more dependable and economical manner (Momenitabar et al., 2020). These evaluations can be further improved by utilizing computer vision and deep learning techniques, particularly in urban settings where comprehensive street-level data may be scarce (Wang, 2024). These methods overcome temporal lags and increase prediction accuracy by extracting pertinent information from sky photos to forecast future PV output (Nie et al., 2023; Misra Palanisamy, 2019). The combination of machine learning and deep learning models can improve short-term solar irradiance forecasts, given the volatility of energy generation due to weather dependence (Carrera et al., 2020) (El-Shahat et al., 2024). A sizable collection of data is frequently used to perform accurate parameter estimation Biswas et al. (2018). This is especially crucial when utilizing evolutionary algorithms to reduce errors and identify the best cell parameters, which may be improved by applying techniques like flower pollination algorithms or particle swarm optimization Biswas et al. (2018).

4. Methodology

Numerical data and mathematical models

The method minimizes inaccuracies in current-voltage relationships at critical points by optimizing all relevant PV cell characteristics without making any assumptions. Biswas et al. (2018).

Mathematical Model

The single-diode and double-diode models are well-established mathematical models that we used in our study to accurately estimate solar cell properties. Our main goal was to make sure that the current-voltage relationships that were obtained from these models accurately reflected the performance at the open circuit, short circuit, and maximum power points Biswas et al. (2018).

For each model, we distinguished between parameters that were optimized by our chosen algorithm and those that were calculated based on fundamental electrical relationships. The specific parameters involved in our modeling approach include the diode ideality factor (a, a_1, a_2), series resistance (R_S), parallel resistance (R_{sh}), photo current (I_L), and diode reverse saturation current (I_0, I_{01}, I_{02}).

The optimized and calculated parameters for each model utilized in our work are summarized in Table 1, drawing inspiration from the parameterization strategies discussed by Biswas et al. (2018):

Table 1: Optimized and Calculated Parameters for PV Models

Model	Optimized Parameters	Calculated Parameters
Single-diode model	$\{a, R_S, R_{sh}\}$	I_L [Eq.], I_0 [Eq.]
Double-diode model	$\{a_1, a_2, R_S, R_{sh}, I_{01}\}$	I_{02} [Eq.], I_L [Eq.]

The formulation of our objective function was critical, and its successful minimization ensured that the derived PV module performance aligned precisely with the empirical I-V characteristics at the three aforementioned major operating points Biswas et al. (2018).

This study's mathematical modeling builds upon foundational research utilizing single-diode and double-diode models. Their work provides an in-depth analysis of comparable circuits for ideal photovoltaic cells and PV modules. Our framework is largely based on their formulations, particularly those explaining the current-voltage behavior.Biswas et al. (2018)

In particular, we build our models using a number of important equations from Biswas et al. (Biswas et al., 2018). These formulas describe how PV cells and modules behave in a variety of scenarios, such as maximum power points, open circuits, and short circuits. As stated in their study, the following formulas are essential to our analysis:

- **The ideal current for PV cells**
  $I = I_{PV,cell} - I_D$ (Biswas et al., 2018)
- **I-V characteristic of ideal PV cell**
  $I = I_{PV,cell} - I_{O,cell}\left[\exp\left(\frac{qV}{akT}\right) - 1\right]$ (Biswas et al., 2018)
- **I-V characteristic of single-diode model for PV module**
  $I = I_{PV} - I_O\left[\exp\frac{q(V+R_S I)}{akN_C T} - 1\right] - \frac{V+R_S I}{R_P}$ (Biswas et al., 2018)
- **Open-circuit condition from single-diode model**
  $0 = I_{PV} - I_O\left[\exp\left(\frac{qV_{OC}}{akN_C T}\right) - 1\right] - \frac{V_{OC}}{R_P}$ (Biswas et al., 2018)
- **Photocurrent (I_{PV}) at open-circuit**
  $I_{PV} = I_O\left[\exp\left(\frac{qV_{OC}}{akN_C T}\right) - 1\right] + \frac{V_{OC}}{R_P}$ (Biswas et al., 2018)
- **Short-circuit condition from single-diode model**
  $I_{SC} = I_{PV} - I_O\left[\exp\left(\frac{qR_S I_{SC}}{akN_C T}\right) - 1\right] - \frac{R_S I_{SC}}{R_P}$ (Biswas et al., 2018)
- **Photocurrent (I_{PV}) at short-circuit**
  $I_{PV} = I_{SC} + I_O\left[\exp\left(\frac{qR_S I_{SC}}{akN_C T}\right) - 1\right] + \frac{R_S I_{SC}}{R_P}$ (Biswas et al., 2018)
- **Reverse saturation current (I_O)**
  $I_O = \frac{I_{SC} + \frac{R_S I_{SC}}{R_P} - \frac{V_{OC}}{R_P}}{\exp\left(\frac{qV_{OC}}{akN_C T}\right) - \exp\left(\frac{qR_S I_{SC}}{akN_C T}\right)}$ (Biswas et al., 2018)
- **Photocurrent (I_{PV}) derived from open and short-circuit conditions**
  $I_{PV} = \left(I_{SC} + \frac{R_S I_{SC}}{R_P} - \frac{V_{OC}}{R_P}\right)\frac{\left[\exp\left(\frac{qV_{OC}}{akN_C T}\right) - 1\right]}{\exp\left(\frac{qV_{OC}}{akN_C T}\right) - \exp\left(\frac{qR_S I_{SC}}{akN_C T}\right)} + \frac{V_{OC}}{R_P}$ (Biswas et al., 2018)
- **Current at maximum power point (I_{MPP})**
  $I_{MPP} = I_{PV} - I_O\left[\exp\frac{q(V_{MPP}+R_S I_{MPP})}{akN_C T} - 1\right] - \frac{V_{MPP}+R_S I_{MPP}}{R_P}$ (Biswas et al., 2018)

In keeping with our concept of mathematical modeling, the double-diode model takes into consideration recombination losses within the depletion region, providing a more accurate depiction of PV module performance. According to Biswas et al., the I-V characteristic equation for a PV module's double-diode model is as follows:

$I = I_{PV} - I_{O1}\left[\exp\frac{q(V+R_S I)}{a_1 kN_C T} - 1\right] - I_{O2}\left[\exp\frac{q(V+R_S I)}{a_2 kN_C T} - 1\right] - \frac{V+R_S I}{R_P}$ (Biswas et al., 2018)

The reverse saturation currents of the two diodes are denoted by I_{O1} and I_{O2} in this equation, while the ideality factors for each are denoted by a_1 and a_2.

An objective function is usually developed for parameter estimation in order to reduce the difference between the model's predictions and the measured data. According to Biswas et al. (Biswas et al., 2018), the goal of optimization is to minimize mistakes at the maximum power points, open circuit, and short circuit. The sum of the squared errors at these three crucial operational points is the aggregate error (ERR) that is employed in their objective function:

$ERR = err_{OC}^2 + err_{SC}^2 + err_{MPP}^2$ (Biswas et al., 2018)

The current-voltage relationships at the open circuit, short circuit, and maximum power points are used to derive these individual error values (err_{OC}, err_{SC}, err_{MPP}) for the double-diode model in a manner similar to that of the single-diode model, specifically referring to equations and the paper (Biswas et al., 2018). At these critical locations, the goal of this optimization is to properly estimate the PV cell parameters so that the I-V characteristics of the model match the actual data (Biswas et al., 2018).

Numerical Data

Our research leveraged comprehensive numerical data for three distinct types of solar cell modules: polycrystalline, monocrystalline, and thin-film, consistent with the module types often characterized in the literature Biswas et al. (2018) . This typical manufacturer-provided data included current and voltage values at the short circuit, open circuit, and maximum power points. All data was acquired under standard test conditions, specifically 25°C and 1000 W/m^2 irradiance. As shown in Table 2.

This analysis is crucial for optimizing solar power generation in varied environmental conditions Chakraborty et al. (2023) Lin and Yu (2025).

5. Application and Validation

Power Output Prediction

By understanding the potential power output, grid operators can make informed decisions about energy dispatch and grid stability Xuan et al. (2024). This facilitates more effective grid management and energy trading strategies Paulescu and Paulescu (2019). It also aids in minimizing the forecasting errors by choosing suitable models and preprocessing methods Robrini et al. (2025) Teixeira et al. (2024).This can lead to improved energy independence and reduced carbon footprints Kalra et al. (2024) T et al. (2024).

6. Case Studies

Japanese Power Utility Case Studies

Japanese electric power companies are actively engaged in promoting renewable energy, aligning with national goals to make renewables a primary power source. Their strategies involve significant investments, organizational restructuring, and adaptation to new market mechanisms.

6.1. Electric Utility Landscape and Market Share

The Japanese power market is primarily dominated by former General Electricity Utilities (10 EPCOs from Hokkaido to Okinawa), which held 81.9% of the market share based on electricity demand in December 2022. Power Producers and Suppliers accounted for the remaining 18.1% Yamazaki and Ikki (2022).

6.2. Renewable Energy Development Targets and Initiatives

Many electric companies have established ambitious targets for renewable energy development and are undergoing internal reorganization to facilitate these goals Yamazaki and Ikki (2022):

The Federation of Electric Power Companies also announced plans to construct large-scale PV power plants with a total capacity of 140 MW, with construction almost completed Yamazaki and Ikki (2022).

6.3. Grid Integration and Challenges

With the expansion of PV installations, challenges related to grid integration have emerged, particularly concerning output curtailment and grid connection:

Yamazaki2022

- **Output Curtailment:** Output curtailment of renewable energy has been conducted, initially in Kyushu in October 2018, and expanded to Hokkaido, Tohoku, Chugoku, and Shikoku areas in 2022. This occurs on weekends and now weekdays due to increased PV penetration Yamazaki and Ikki (2022). The Organization for Cross-regional Coordination of Transmission Operators, JAPAN, verifies the appropriateness of this curtailment Yamazaki and Ikki (2022).

- **Grid Connection Policies:** Some electric companies temporarily suspended responses to new grid connection applications in 2014 due to the growth of PV capacity. They then introduced a limit of 30 days/year or 360 hours/year for output curtailment to manage grid capacity Yamazaki and Ikki (2022).

- **Grid Enhancement:**Efforts are underway to enhance interregional grid connection lines to transport electricity from areas with abundant renewable energy resources to demand centers. This includes frequency conversion stations and a master plan for wide-area interconnection systems Yamazaki and Ikki (2022). A new wheeling scheme, the "revenue cap system," is scheduled for introduction in FY 2023, which is expected to increase wheeling charges in various regions Yamazaki and Ikki (2022).

6.4. New Business Models and Partnerships

Electric companies are also adapting to new business models to integrate more renewable energy:

- **Corporate Power Purchase Agreements:** Both on-site and off-site Corporate PPA schemes are progressing, targeting electricity users and large customers, driven by rising electricity bills Yamazaki and Ikki (2022).

- **Self-Consumption:** Electric companies are advancing activities to promote self-consumption of PV electricity, especially for residential PV systems whose Feed-in Tariff purchase period has terminated Yamazaki and Ikki (2022).

- **Surplus Electricity Purchase:** Electric companies and Power Producers and Suppliers offer purchase menus for surplus electricity from post-FIT residential PV systems Yamazaki and Ikki (2022)

These points highlight the significant role Japanese power utilities play in the country's renewable energy transition, addressing both technical and market-related challenges.

Table 2: Electrical parameters for the PV cells at standard test conditions (STC).

Parameter	KC200GT (K.C. (2004))	SQ85 (Soon et al. (2012))	ST40 (Soon et al. (2012))
Type	Polycrystalline	Monocrystalline	Thin film
Open circuit voltage, V_{OC} (volt)	32.9	22.20	23.30
Short circuit current, I_{SC} (amp)	8.21	5.45	2.68
Voltage at maximum power, V_{MPP} (volt)	26.3	17.20	16.60
Current at maximum power, I_{MPP} (amp)	7.61	4.95	2.41
Temperature coefficient of V_{OC}, $K_{V,OC}$ (volt/°C)	-0.123	-0.0725	-0.1
Temperature coefficient of I_{SC}, $K_{I,SC}$ (amp/°C)	3.18×10^{-3}	0.8×10^{-3}	0.35×10^{-3}
Number of cells in series, N_C	54	36	36

Table 3: Renewable Energy Targets by Japanese Electric Utilities

Utility	Renewable Energy Target	Notes
Hokkaido Electric Power	>300 MW increase in renewable energy capacity in Hokkaido and other regions by 2030; carbon neutral by 2050	Established Renewable Energy Development Promotion Department (Yamazaki and Ikki, 2022)
Tohoku Electric	2 GW renewable energy target as early as 2030 onwards	Established Corporate PPA Office (Yamazaki and Ikki, 2022)
Chubu Electric	>3.2 GW renewable energy development by 2030	Formulated ”Chubu Electric Power Group Management Vision 2.0” (Yamazaki and Ikki, 2022)
Hokuriku Electric	Accelerate renewable energy development to achieve ”Hokuriku Electric Power Group 2030 Long-term Vision”	Established Renewable Energy Department (Yamazaki and Ikki, 2022)
Kansai Electric Power	Invest 340 BJPY in renewable energy-related projects	Formulated ”Kansai Electric Power Group Medium-term Management Plan (2021–2025)” (Yamazaki and Ikki, 2022)
Chugoku Electric	300 to 700 MW renewable energy by FY 2030; carbon neutrality by 2050	Under group management vision ”Energia Change 2030” (Yamazaki and Ikki, 2022)
Shikoku Electric	500 MW by FY 2030 and 2 GW by FY 2050; carbon neutrality by 2050	Focusing on new development of renewable energy (Yamazaki and Ikki, 2022)
Okinawa Electric	Invest about 6 BJPY by FY 2025	Increase installed capacity of renewable energy and upgrade grid stabilization technology using storage batteries (Yamazaki and Ikki, 2022)
TEPCO Renewable Power	Succeeded approximately 10 GW of renewable energy power sources; aims to develop 6–7 GW by mid-2030s	Includes hydro, wind, and PV projects in Japan and abroad (Yamazaki and Ikki, 2022)

7. Discussion

The method combines analytical and metaheuristic approaches to optimize parameters for both single- and double-diode models, ensuring all PV cell parameters are optimized without presumptions Biswas et al. (2018). This enhances the accuracy of PV system simulations, especially in environments with limited data Biswas et al. (2018).
This is accomplished by reducing the discrepancy between the PV system's simulated and experimental I-V data Biswas et al. (2018). Additionally, this makes it easier to design and manage both independent and grid-connected PV systems Biswas et al. (2018). This method provides a workable solution for performance prediction and optimization, and is especially beneficial in situations where comprehensive experimental data is not available Biswas et al. (2018). These techniques can offer more dependable and economical grid integration of solar electricity (Guo et al., 2020) (Ascencio-Vázquez et al., 2020). Ultimately, the created model boosts the financial return of solar installations both on and off the grid by providing a simplified method for improving energy output estimations and fine-tuning inverter designs (Guo et al., 2020) (Khan et al., 2021).

To validate our models and present our findings, we generated several tables and figures within our study, mirroring the comprehensive reporting standards found in Biswas et al. (2018):

8. Results

All experiments were conducted on AMD Ryzen 7 7730U with Radeon Graphics (2.00 GHz) with 16.0 GB RAM (13.8 GB usable) running 64-bit operating system.

8.1. Parameter Estimation Results

All three algorithms successfully extracted PV parameters satisfying I-V relationships at three critical operating points. Key findings include photovoltaic currents that aligned with theoretical expectations: KC200GT (8.21–8.37 A), Shell SQ85 (5.45–5.56 A), and Shell ST40 (2.68–2.73 A). Series resistance optimization frequently achieved $R_s = 0.0010\ \Omega$ boundary constraint, and multiple optimal solutions were confirmed for each material, validating theoretical assertions about solution non-uniqueness. Material-specific performance analysis revealed that KC200GT (polycrystalline) exhibited the highest current generation capacity with consistent optimization across algorithms, Shell SQ85 (monocrystalline) demonstrated intermediate performance characteristics, while Shell ST40 (thin-film) showed the lowest current generation with significant algorithmic performance variations.

Table 4: Statistical summary of optimization results with different algorithms

Case no.	**Algorithm**	**Error function (ERR)**				**Total CPU time**
		Best	**Worst**	**Mean**	**Std. dev.**	**(sec.)**
KC200GT (Single-diode model)	GA	0	0	0	0	70.6
	PSO	0	0	0	0	18.1
	ABC	0	5.61×10^{11}	4.73×10^{12}	1.19×10^{11}	110.3
	MSA	0	0	0	0	50.8
	GWO	0	2.79×10^{11}	5.27×10^{12}	7.80×10^{12}	8.2
	L-SHADE	0	0	0	0	17.9
	BWR(Rao (2024))	0	0	0	0	**2.01**
	BMR(Rao (2024))	0	0	0	0	**2.16**
	Jaya(Rao (2016))	0	0	0	0	**0.79**
KC200GT (Double-diode model)	GA	0	0	0	0	85.5
	PSO	0	0	0	0	21.7
	ABC	0	5.79×10^{11}	4.84×10^{12}	1.05×10^{11}	150.7
	MSA	0	0	0	0	65.4
	GWO	0	9.86×10^{11}	5.51×10^{12}	1.82×10^{11}	10.9
	L-SHADE	0	0	0	0	18.6
	BWRRao (2024)	0	0	0	0	**1.44**
	BMRRao (2024)	0	0	0	0	**3.58**
	JayaRao (2016)	0	0	0	0	**1.37**

Table 5: Optimized parameters for single-diode model using BWR, BMR, and JAYA algorithms

Material	**Algorithm**	a	R_s **(Ω)**	R_p **(Ω)**	I_o (A)	I_{pv} (A)	**ERR (mean)**	**CPU (s)**
KC200GT	BWR	1.0273	0.0010	50.0000	7.13×10^{1}	8.2102	0	2.01
KC200GT	BMR	1.0273	0.0010	50.0000	7.13×10^{1}	8.2102	0	2.16
KC200GT	JAYA	1.0273	0.0010	50.0000	7.13×10^{1}	8.2102	0	0.79
Shell SQ85	BWR	1.5570	0.0010	50.0000	1.01×10	5.4501	0	2.14
Shell SQ85	BMR	2.0000	0.0010	117.3648	3.23×10	5.4500	0	2.16
Shell SQ85	JAYA	2.0000	0.0010	117.3639	3.23×10	5.4500	0	0.21
Shell ST40	BWR	0.7823	0.2835	61.3265	2.39×10^{1}	2.6924	0	0.88
Shell ST40	BMR	1.8161	0.0853	61.5221	2.33×10	2.7336	0	0.05
Shell ST40	JAYA	2.0000	0.3740	101.2313	8.33×10	2.6899	0	1.46

Table 6: Optimized parameters for double-diode model using BWR, BMR, and JAYA algorithms

Material	**Algorithm**	a_1	a_2	R_s (Ω)	R_p (Ω)	I_{o1} **(A)**	I_{o2} **(A)**	I_{pv} **(A)**	**ERR (mean)**	**CPU (s)**
KC200GT	BWR	1.2784	1.0344	0.2192	74.9367	8.05×10^{-12}	8.05×10^{-11}	8.3742	0	1.44
KC200GT	BMR	1.0442	0.7540	0.0024	50.0166	9.41×10^{-10}	9.41×10^{-9}	8.3742	0	3.58
KC200GT	JAYA	1.0911	0.5008	0.0510	50.0146	1.64×10^{-9}	1.64×10^{-8}	8.3742	0	1.37
Shell SQ85	BWR	1.9181	1.5487	0.0082	50.1358	1.30×10^{-9}	1.30×10^{-8}	5.5590	0	3.36
Shell SQ85	BMR	1.2354	0.7562	0.5196	50.1373	1.95×10^{-10}	1.95×10^{-9}	5.5590	0	3.49
Shell SQ85	JAYA	1.9625	1.9985	0.0013	116.9369	4.60×10^{-8}	4.60×10^{-7}	5.5590	0	0.35
Shell ST40	BWR	1.3204	1.2444	0.6085	67.1851	6.46×10^{-10}	6.46×10^{-9}	2.7336	0	3.18
Shell ST40	BMR	1.7336	0.7306	0.2492	61.2966	1.10×10^{-10}	1.10×10^{-9}	2.7336	0	3.43
Shell ST40	JAYA	1.9288	1.9906	0.0015	80.1476	1.10×10^{-8}	1.10×10^{-7}	2.7336	0	0.07

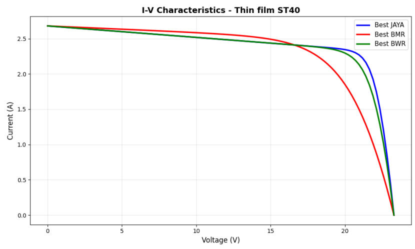

(a) IV Curves

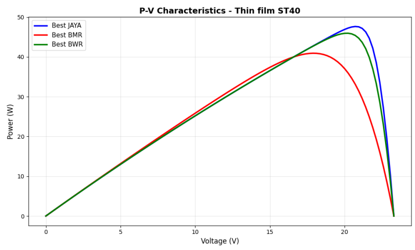

(b) PV Curves

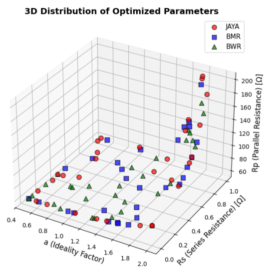

(c) Parameter Distribution

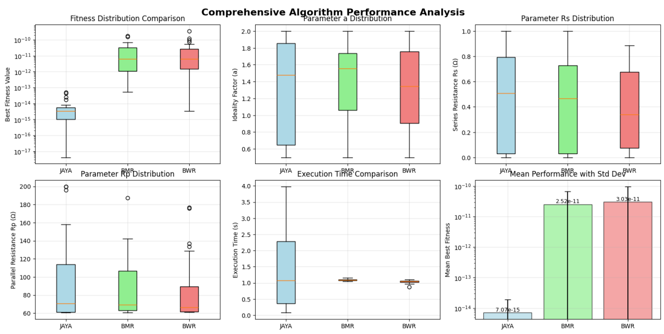

(d) Performance Analysis

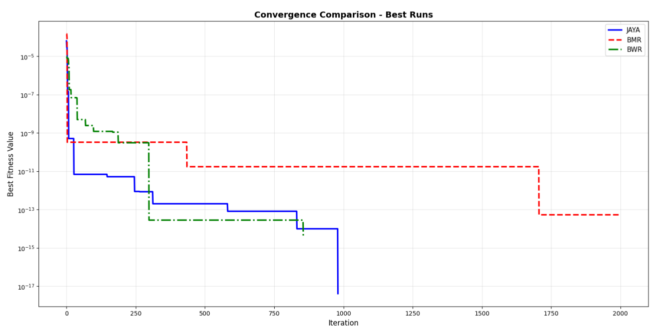

(e) Convergence Curve

Figure 1: Graphical Visualization of Single-Diode (Shell ST40) Behavior Using BWR, BMR and JAYA Optimization Algorithm

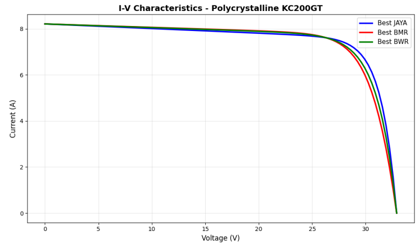

(a) IV Curves

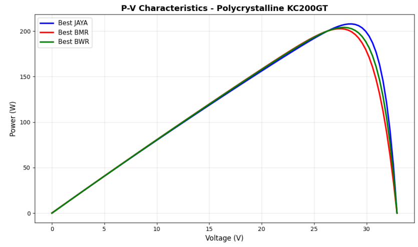

(b) PV Curves

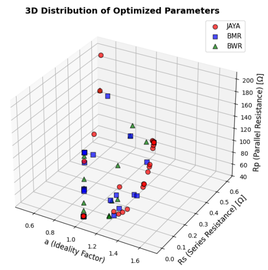

(c) Parameter Distribution

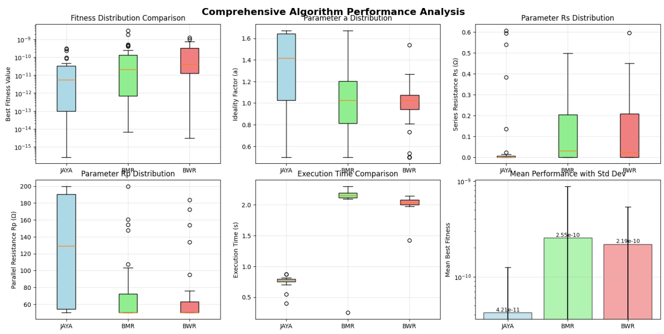

(d) Performance Analysis

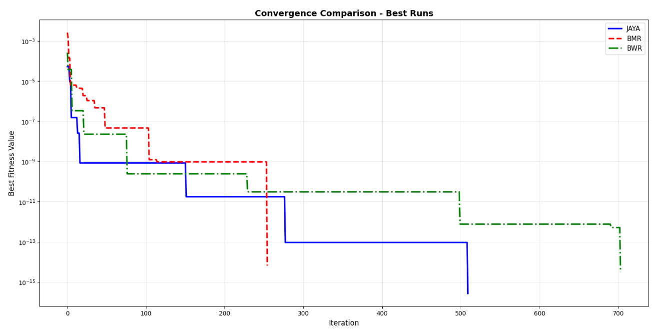

(e) Convergence Curve

Figure 2: Graphical Visualization of Single-Diode (KC400GT) Behavior Using BWR, BMR and JAYA Optimization Algorithm

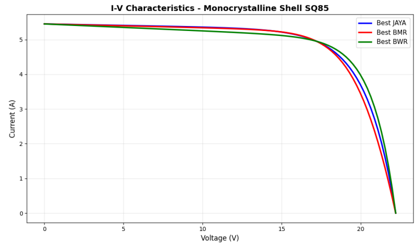

(a) IV Curves

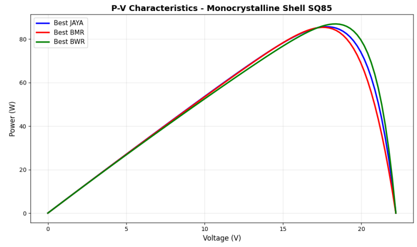

(b) PV Curves

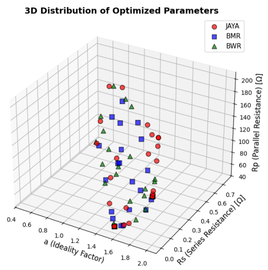

(c) Parameter Distribution

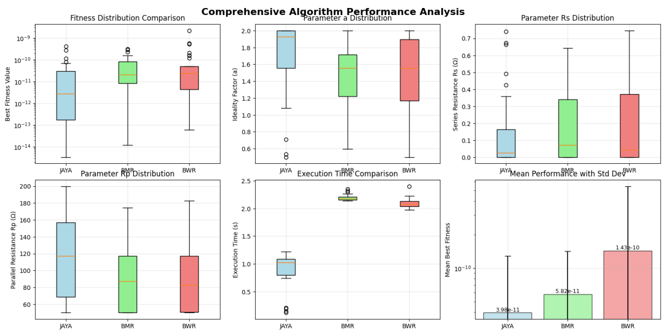

(d) Performance Analysis

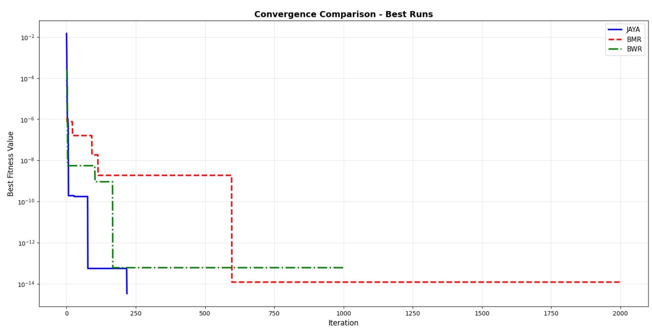

(e) Convergence Curve

Figure 3: Graphical Visualization of Single-Diode (Shell SQ85) Behavior Using BWR, BMR and JAYA Optimization Algorithm

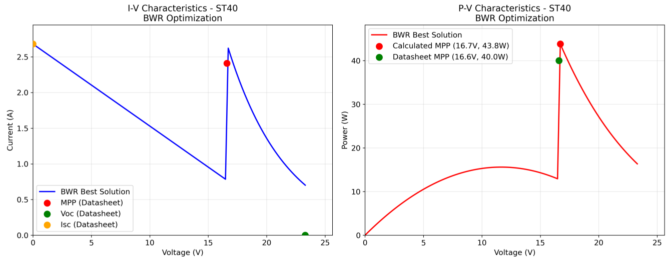

(a) IV and PV Curves

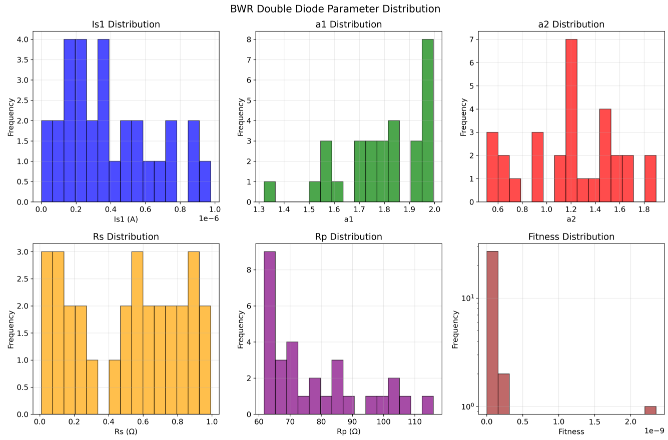

(b) Parameter Distribution

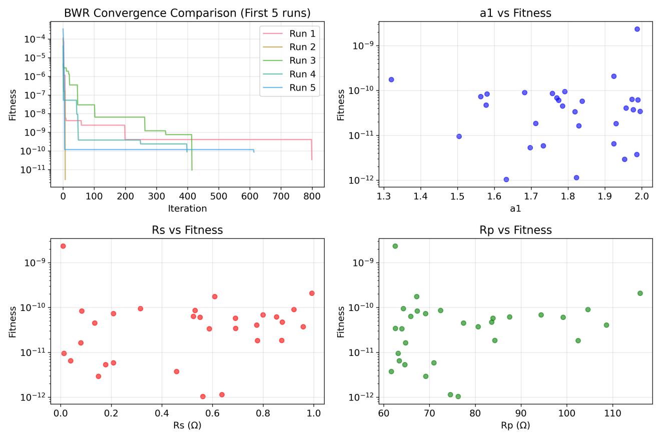

(c) Statistical Analysis

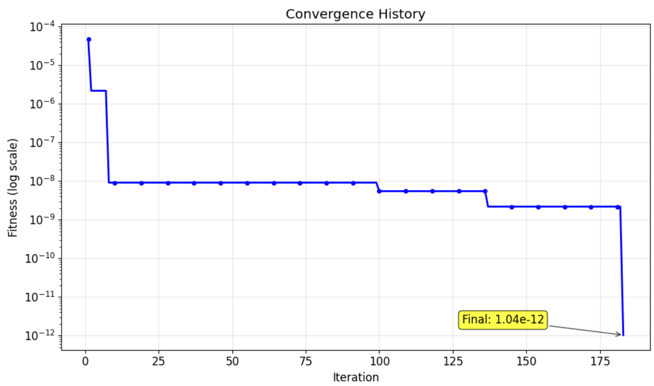

(d) BWR Shell ST40

Figure 4: Graphical Visualization of Double-Diode (Shell ST40) Behavior Using BWR Optimization Algorithm

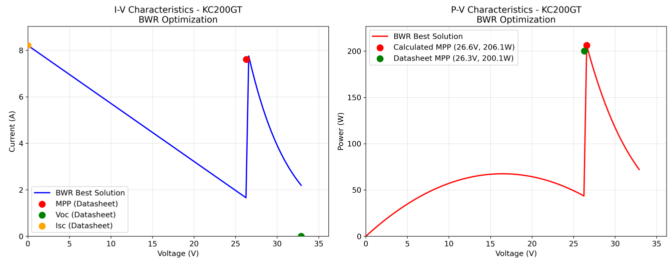

(a) IV and PV Curves

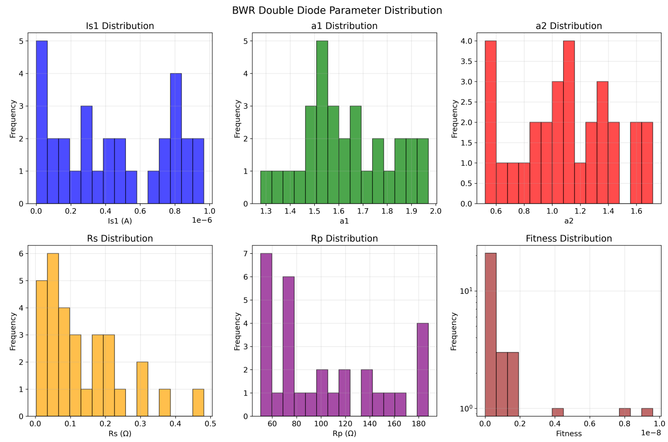

(b) Parameter Distribution

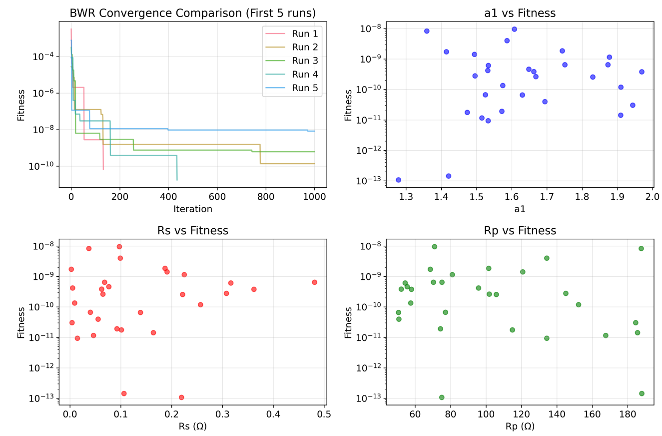

(c) Statistical Analysis

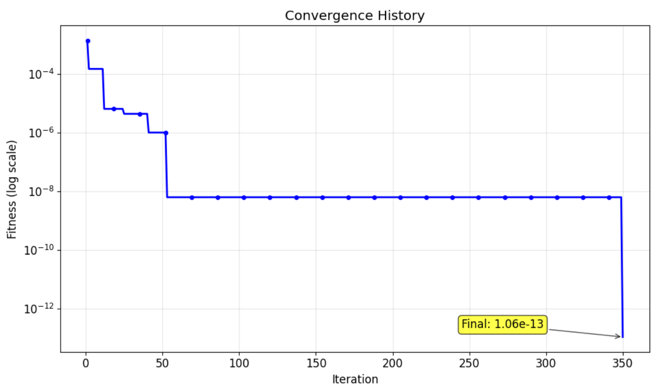

(d) BWR KC200GT

Figure 5: Graphical Visualization of Double-Diode (KC200GT) Behavior Using BWR Optimization Algorithm

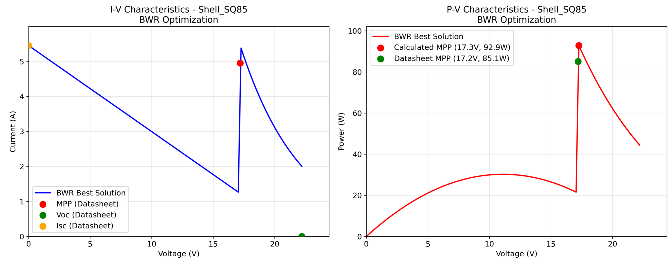

(a) IV and PV Curves

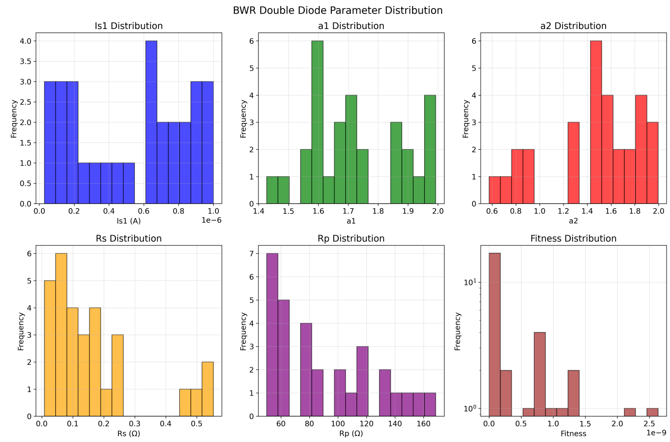

(b) Parameter Distribution

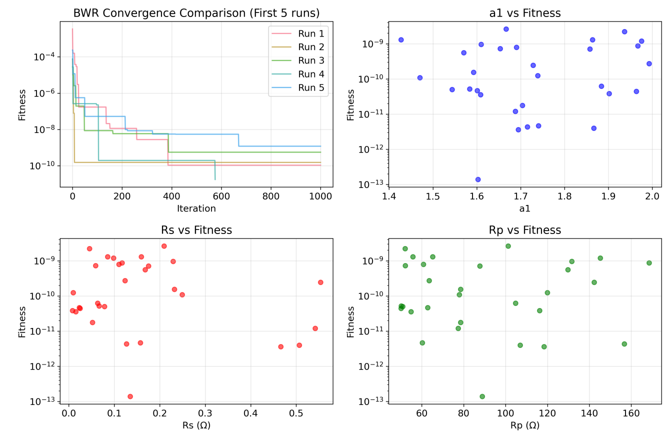

(c) Statistical Analysis

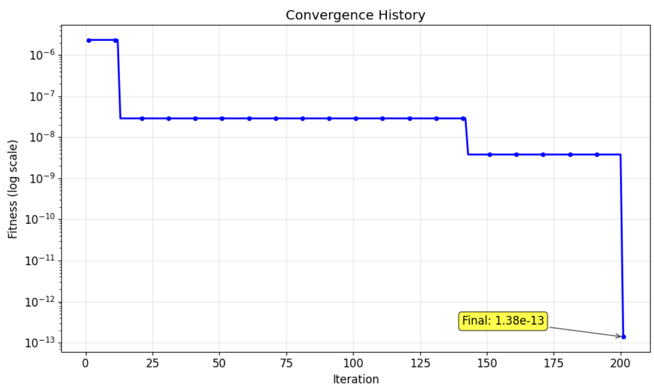

(d) BWR Shell SQ85

Figure 6: Graphical Visualization of Double-Diode (Shell SQ85) Behavior Using BWR Optimization Algorithm

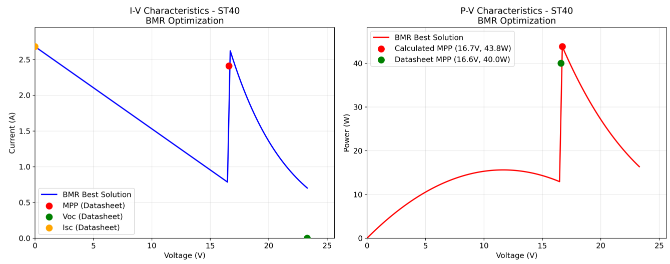

(a) IV and PV Curves

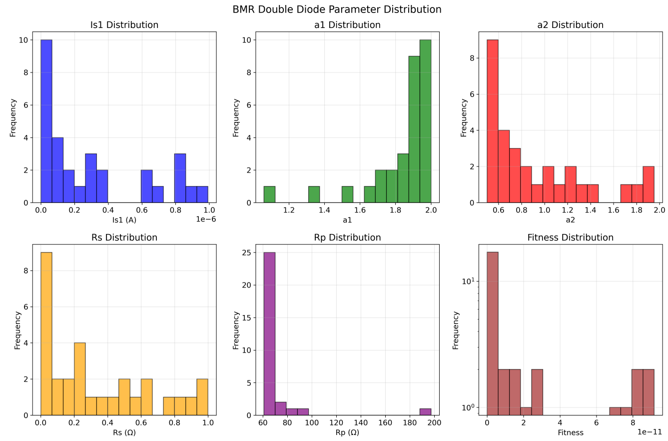

(b) Parameter Distribution

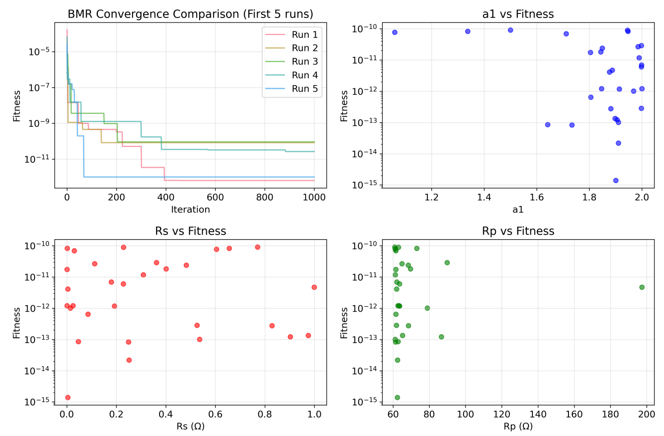

(c) Statistical Analysis

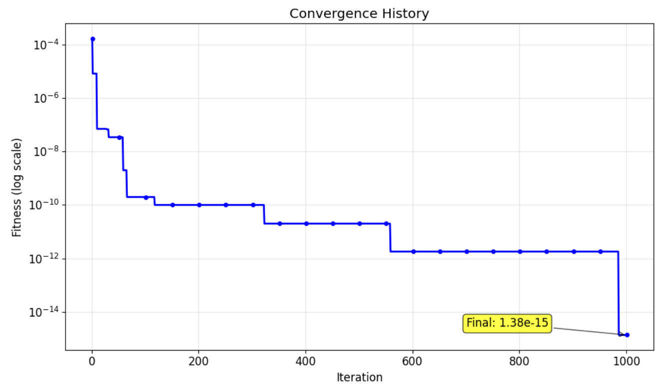

(d) BMR Shell ST40

Figure 7: Graphical Visualization of Double-Diode (Shell ST40) Behavior Using BMR Optimization Algorithm

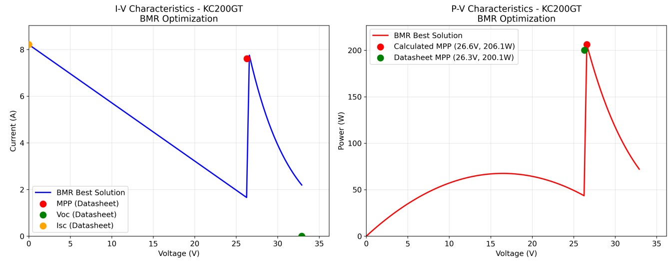

(a) IV and PV Curves

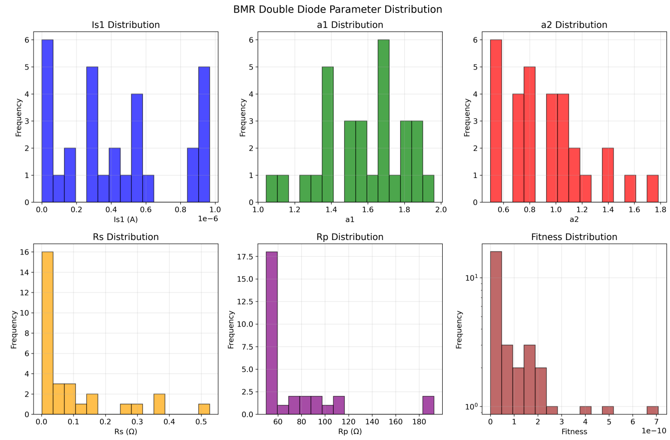

(b) Parameter Distribution

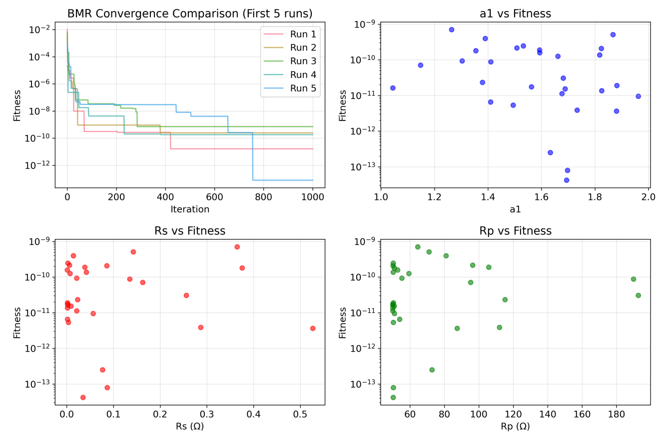

(c) Statistical Analysis

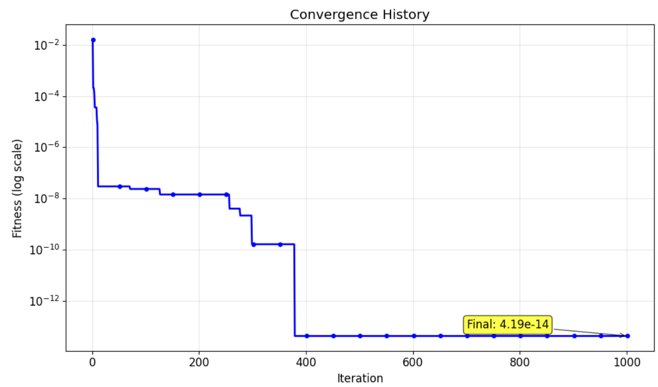

(d) BMR KC400GT

Figure 8: Graphical Visualization of Double-Diode (KC200GT) Behavior Using BMR Optimization Algorithm

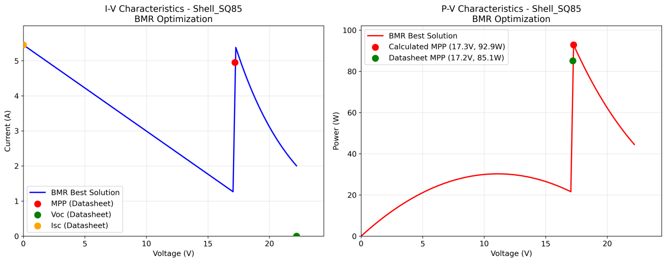

(a) IV and PV Curves

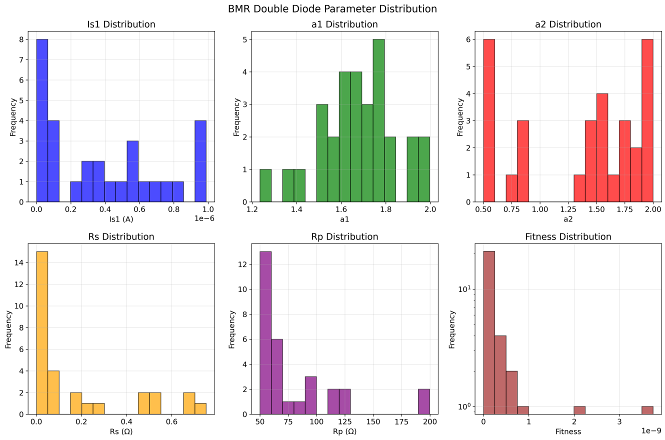

(b) Parameter Distribution

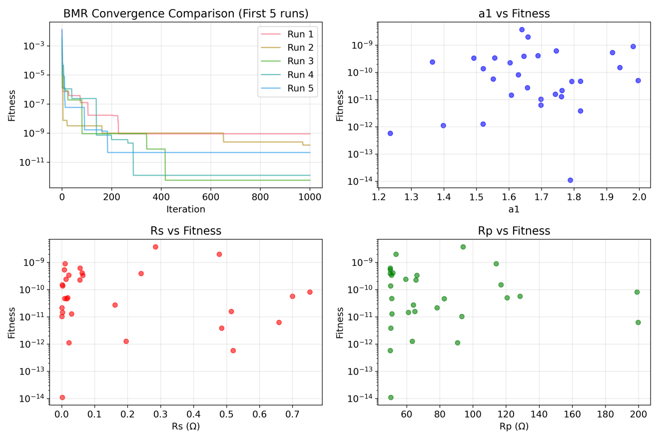

(c) Statistical Analysis

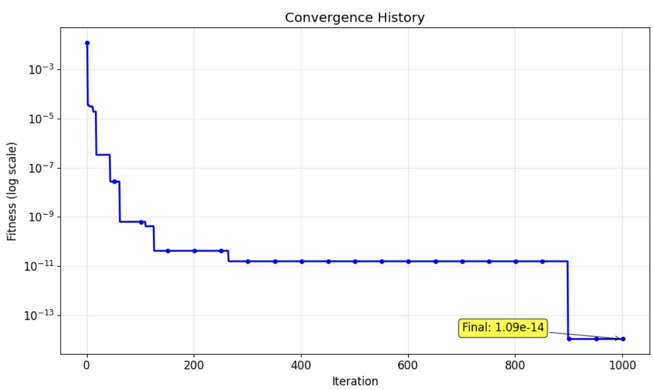

(d) BMR Shell SQ85

Figure 9: Graphical Visualization of Double-Diode (Shell SQ85) Behavior Using BMR Optimization Algorithm

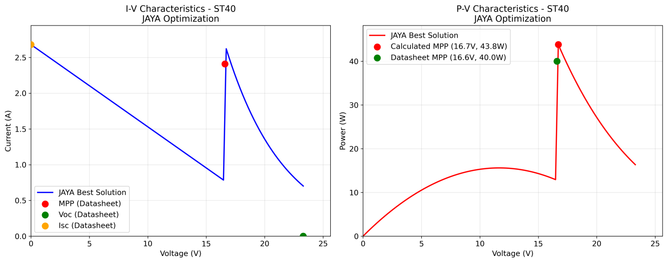

(a) IV and PV Curves

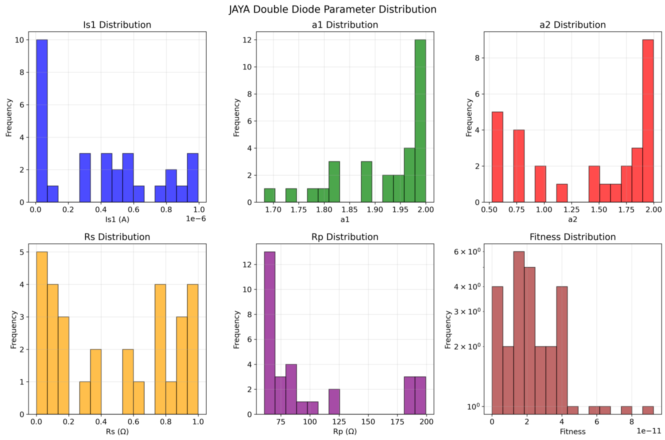

(b) Parameter Distribution

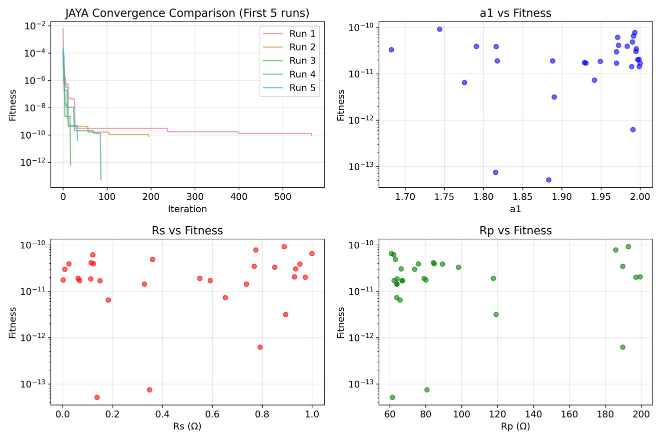

(c) Statistical Analysis

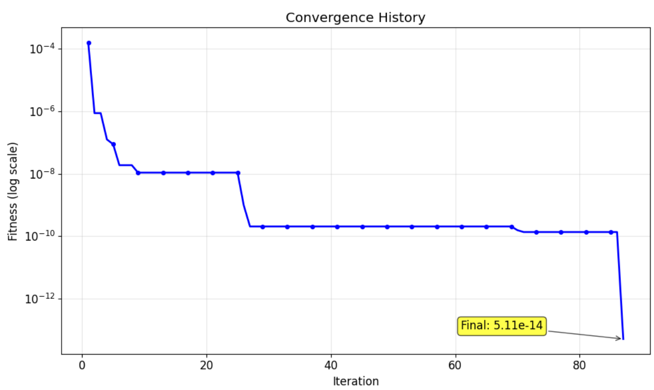

(d) JAYA Shell ST40

Figure 10: Graphical Visualization of Double-Diode (Shell ST40) Behavior Using JAYA Optimization Algorithm

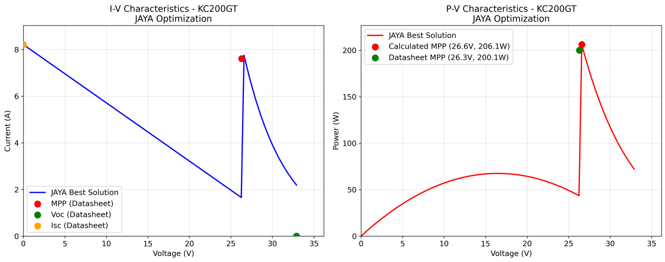

(a) IV and PV Curves

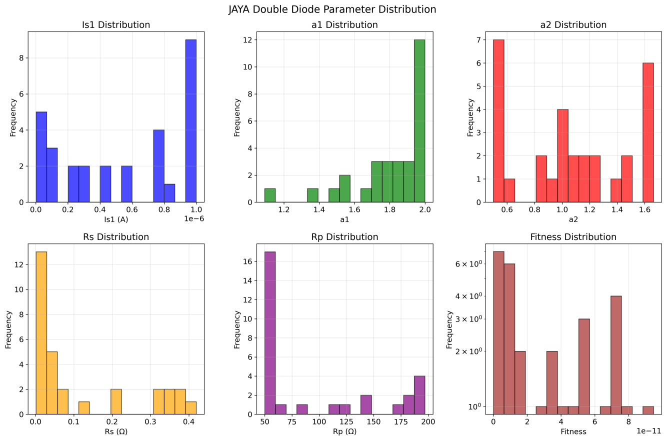

(b) Parameter Distribution

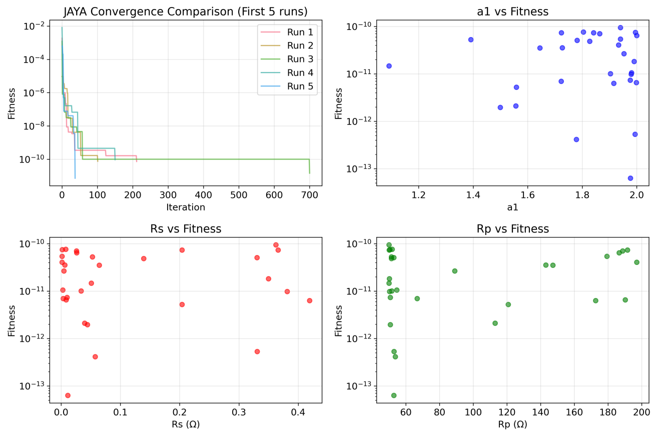

(c) Statistical Analysis

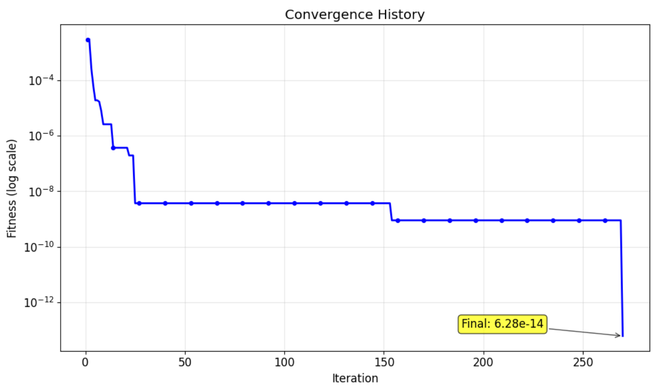

(d) JAYA KC400GT

Figure 11: Graphical Visualization of Double-Diode (KC400GT) Behavior Using JAYA Optimization Algorithm

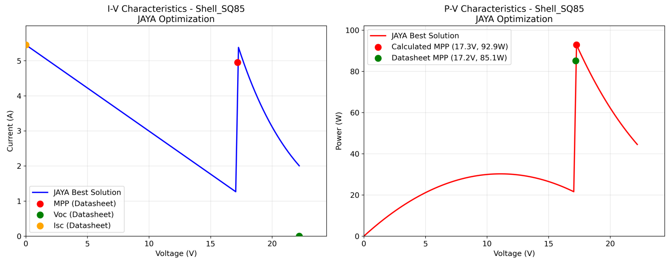

(a) IV and PV Curves

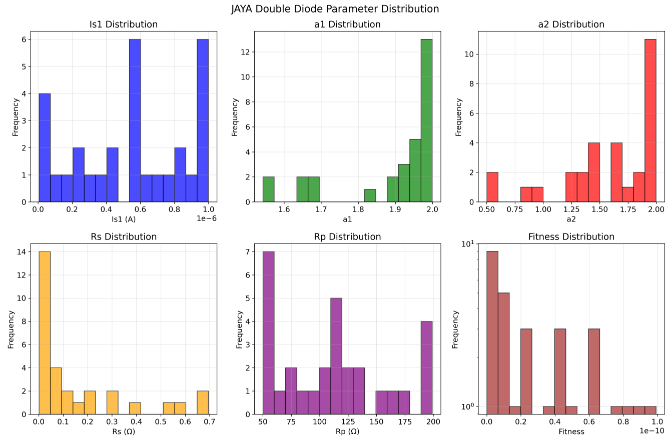

(b) Parameter Distribution

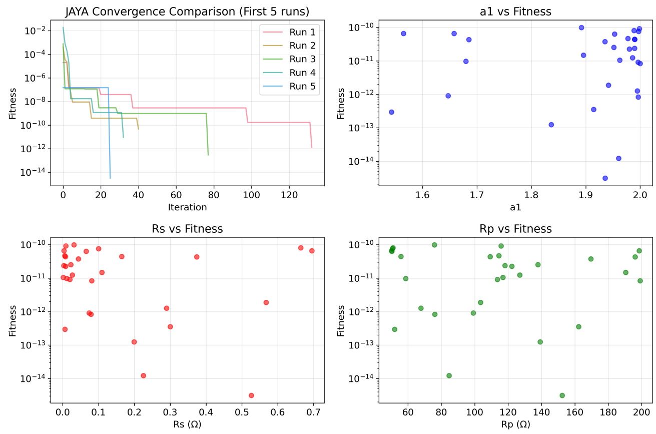

(c) Statistical Analysis

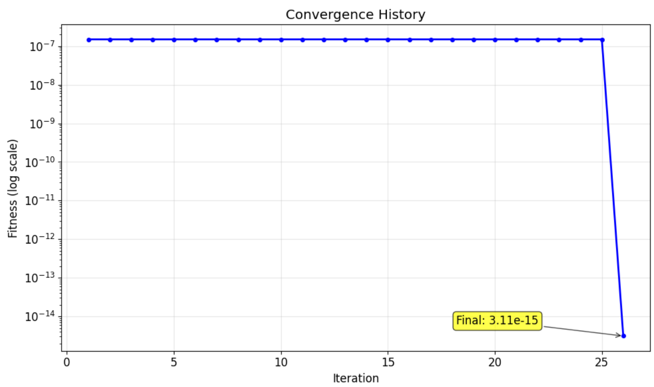

(d) JAYA Shell SQ85

Figure 12: Graphical Visualization of Double-Diode (Shell SQ85) Behavior Using JAYA Optimization Algorithm

9. Conclusion

This study successfully validates three metaheuristic algorithms (BWR, BMR, JAYA) for PV parameter estimation using limited datasheet information. JAYA algorithm emerges as the most computationally efficient solution, achieving convergence up to 20 times faster than competing methods while maintaining solution quality.

The research confirms that multiple parameter sets can satisfy datasheet constraints, providing design flexibility but requiring careful parameter selection based on application needs. All algorithms demonstrated reliable parameter extraction capabilities, supporting accurate PV modeling for grid integration and energy forecasting applications.

The demonstrated computational efficiency makes these methods suitable for real-time applications in Japan's smart grid infrastructure, directly supporting the nation's 120 GW PV capacity target by 2030 through enhanced system modeling and operational planning capabilities.

References

A. Assaf, H. Haron, H. N. A. Hamed, F. A. Ghaleb, S. N. Qasem, and A. M. Albarrak. A review on neural network based models for short term solar irradiance forecasting. *Applied Sciences*, 13(14):8332, 2023. doi: 10.3390/app13148332.

P. P. Biswas, P. N. Suganthan, G. Wu, and G. A. J. Amaratunga. Parameter estimation of solar cells using datasheet information with the application of an adaptive differential evolution algorithm. *Renewable Energy*, 132:425, 2018. doi: 10.1016/j.renene.2018.07.152.

B. Carrera, M. K. Sim, and J. Jung. Pvhybnet: a hybrid framework for predicting photovoltaic power generation using both weather forecast and observation data. *IET Renewable Power Generation*, 14(12):2192, 2020. doi: 10.1049/iet-rpg.2018.6174.

D. Chakraborty, J. Mondal, H. B. Barua, and A. Bhattacharjee. Computational solar energy – ensemble learning methods for prediction of solar power generation based on meteorological parameters in eastern india. arXiv (Cornell University), 2023.

D. Chen and D. Irwin. Black-box solar performance modeling. *ACM SIGMETRICS Performance Evaluation Review*, 45(2):79, 2017. doi: 10.1145/3152042.3152067.

T. Gayibov and E. Abdullaev. Optimization of daily operation mode of photovoltic systems of enterprises. In *E3S Web of Conferences*, volume 264, page 4063, 2021. doi: 10.1051/e3sconf/202126404063.

M. Hopwood and T. Gunda. Generation of data-driven expected energy models for photovoltaic systems. *Applied Sciences*, 12(4):1872, 2022. doi: 10.3390/app12041872.

K. J. Iheanetu. Solar photovoltaic power forecasting: A review. *Sustainability*, 14(24):17005, 2022. doi: 10.3390/su142417005.

X. Jiang, M. Jiang, and Q. Zhou. Day-ahead pv power forecasting based on mstl-tft. arXiv (Cornell University), 2023.

S. Kalra, R. Beniwal, V. P. Singh, and N. S. Beniwal. Innovative approaches in residential solar electricity: Forecasting and fault detection using machine learning. *Electricity*, 5(3):585, 2024. doi: 10.3390/electricity5030029.

K.C. *KC200GT High Efficiency Multicrystal Photovoltaic Module Datasheet*. Kyocera Corporation, 2004. [Online]. Available: `http://www.kyocerasolar.com/assets/001/5195.pdf`.

B. Kim, D. Suh, M.-O. Otto, and J.-S. Huh. A novel hybrid spatio-temporal forecasting of multisite solar photovoltaic generation. *Remote Sensing*, 13 (13):2605, 2021. doi: 10.3390/rs13132605.

D. L. King, W. E. Boyson, and J. A. Kratochvil. Analysis of factors influencing the annual energy production of photovoltaic systems. In *Photovoltaic Specialists Conference*, volume 1356, 2003. doi: 10.1109/pvsc.2002.1190861.

R. Kohút and M. Kvasnica. Power output reconstruction of photovoltaic curtailment. Zenodo (CERN European Organization for Nuclear Research), 2023.

M. Konstantinou, S. Peratikou, and A. G. Charalambides. Solar photovoltaic forecasting of power output using lstm networks. *Atmosphere*, 12(1):124, 2021. doi: 10.3390/atmos12010124.

A. Kumar, A. K. Dubey, I. S. Ramírez, A. M. del Río, and F. P. G. Márquez. Artificial intelligence techniques for the photovoltaic system: A systematic review and analysis for evaluation and benchmarking. *Archives of Computational Methods in Engineering*, 2024. doi: 10.1007/s11831-024-10125-3.

D. S. Kumar, G. M. Yagli, M. Kashyap, and D. Srinivasan. Solar irradiance resource and forecasting: a comprehensive review. *IET Renewable Power Generation*, 14(10):1641, 2020. doi: 10.1049/iet-rpg.2019.1227.

A. J. Lari, A. Sanfilippo, D. Bachour, and D. Pérez-Astudillo. Using machine learning algorithms to forecast solar energy power output. *Electronics*, 14 (5):866, 2025. doi: 10.3390/electronics14050866.

P. D. Leo, A. Ciocia, G. Malgaroli, and F. Spertino. Advancements and challenges in photovoltaic power forecasting: A comprehensive review. Preprints, 2025.

H. Li, J. Li, and Y. Mi. Research on photovoltaic power prediction technology based on machine learning. In *Journal of Physics Conference Series*, volume 2087, page 12004, 2021. doi: 10.1088/1742-6596/2087/1/012004.

W. Liao, B. Bak-Jensen, J. R. Pillai, Z. Yang, and K. Liu. Short-term power prediction for renewable energy using hybrid graph convolutional network and long short-term memory approach. *Electric Power Systems Research*, 211:108614, 2022. doi: 10.1016/j.epsr.2022.108614.

H. Lin and M. Yu. A novel distributed pv power forecasting approach based on time-llm. arXiv (Cornell University), 2025.

S. Meisenbacher, B. Heidrich, T. Martin, R. Mikut, and V. Hagenmeyer. Autopv: Automated photovoltaic forecasts with limited information using an ensemble of pre-trained models. arXiv (Cornell University), 2022.

Y. Mhanni and Y. Lagmich. Maximizing solar panel efficiency in partial shade: The improved poa solution for mppt. *International Journal of Advanced Computer Science and Applications*, 15(3), 2024. doi: 10.14569/ijacsa.2024.0150397.

D. H. Muhsen, T. Khatib, and F. Nagi. A review of photovoltaic water pumping system designing methods, control strategies and field performance. *Renewable and Sustainable Energy Reviews*, 68:70, 2016. doi: 10.1016/j.rser.2016.09.129.

T. N. L. Nguyen and F. Müsgens. What drives the accuracy of pv output forecasts? arXiv (Cornell University), 2021.

M. Paulescu and E. Paulescu. Short-term forecasting of solar irradiance. *Renewable Energy*, 143:985, 2019. doi: 10.1016/j.renene.2019.05.075.

Rao. Bmr and bwr: Two simple metaphor-free optimization algorithms for solving real-life non-convex constrained and unconstrained problems. 2024. doi: 10.48550/arXiv.2407.11149.

R. Venkata Rao. Jaya: A simple and new optimization algorithm for solving constrained and unconstrained optimization problems. *International Journal of Industrial Engineering Computations*, 7(1):19–34, 2016. doi: 10.5267/j.ijiec.2015.8.004.

A. Rashid. Nano fullerenes with the ability to store electrostatic energy that can be used as nano supercapacitors with very high capacity. ResearchGate, 2024.

H. Riggs, S. Tufail, M. Tariq, and A. I. Sarwat. Combined machine learning and physics-based forecaster for intra-day and 1-week ahead solar irradiance forecasting under variable weather conditions. arXiv (Cornell University), 2023.

F. E. Robrini, B. Amrouche, Ü. Cali, and T. S. Ustun. Assessment of machine and deep learning models integrated with variational mode decomposition for photovoltaic power forecasting using real-world data from the semi-arid region of djelfa, algeria. *Energy Conversion and Management X*, page 101108, 2025. doi: 10.1016/j.ecmx.2025.101108.

N. Salazar-Peña, A. Tabares, and A. González-Mancera. Ai-powered dynamic fault detection and performance assessment in photovoltaic systems. SSRN, 2024.

S. Soleymani and S. Mohammadzadeh. Comparative analysis of machine learning algorithms for solar irradiance forecasting in smart grids. arXiv (Cornell University), 2023.

Soon et al. Photovoltaic model identification using particle swarm optimization with inverse barrier constraint. *IEEE Transactions on Power Electronics*, 27 (9):3975–3983, 2012. doi: 10.1109/TPEL.2012.2190524.

M. R. A. T, B. S. Balaji, S. A. P. R. R, C. Rani, R. K. M, P. Ramachandran, S. Rajkumar, V. N. Kumar, G. Aggarwal, and A. M. Siddiqui. Intelligent energy management across smart grids deploying 6g iot, ai, and blockchain in sustainable smart cities. *IoT*, 5(3):560, 2024. doi: 10.3390/iot5030025.

R. Teixeira, A. Cerveira, E. J. S. Pires, and J. Baptista. Advancing renewable energy forecasting: A comprehensive review of renewable energy forecasting methods. *Energies*, 17(14):3480, 2024. doi: 10.3390/en17143480.

N. Ulapane, S. G. Abeyratne, P. Binduhewa, C. H. Dhanapala, S. Wickramasinghe, and N. Rathnayake. A simple software application for simulating commercially available solar panels. *International Journal of Soft Computing and Software Engineering [JSCSE]*, 2(5):48, 2012. doi: 10.7321/jscse.v2.n5.5.

Y. Xuan, Y. Dong, and T. Wu. Short-term forecasting of photovoltaic power generation based on entropy during the foggy winter. arXiv (Cornell University), 2024.

M. Yamazaki and O. Ikki. *National Survey Report of PV Power Applications in Japan 2022*. IEA PVPS Programme, 2022. doi: 10.54550/iea.pvps.

X. Zhang, R. Shen, and Y. Wang. A combined method of two-model based on forecasting meteorological data for photovoltaic power generation forecasting. In *E3S Web of Conferences*, volume 185, page 1053, 2020. doi: 10.1051/e3sconf/202018501053.

A. BWR Algorithm

A.1. Single-Diode Model

A.1.1. Shell ST40 (Thin-Film)

Table A.7: Optimal parameters for single-diode model of *Shell ST40* using BWR.

Run	a	R_s ()	R_p ()	I_0 (A)	I_{pv} (A)	ERR	Time(s)
1	2.0000	0.0010	80.5745	8.10e-06	2.6800	0	1.04
2	0.5000	0.0453	61.4372	3.03e-22	2.6820	0	1.03
3	1.1652	0.6974	66.2752	9.62e-10	2.7082	0	1.02
4	1.7390	0.8162	118.6287	1.28e-06	2.6984	0	1.07
5	1.3734	0.8168	77.2805	2.60e-08	2.7083	0	1.06
6	0.7934	0.0279	61.5178	3.74e-14	2.6812	0	1.07
7	1.2901	0.0010	63.4647	7.65e-09	2.6800	0	1.05
8	1.5205	0.1357	67.6611	1.49e-07	2.6854	0	1.09
9	1.0326	0.1976	62.0696	5.87e-11	2.6885	0	1.10
10	1.8837	0.8498	176.6673	3.99e-06	2.6929	0	1.01
11	0.5000	0.3840	61.0993	3.05e-22	2.6968	0	1.04
12	1.2876	0.3211	65.0431	7.44e-09	2.6932	0	1.04
13	0.5000	0.2220	61.2591	3.04e-22	2.6897	0	1.00
14	1.4794	0.0548	66.1225	9.38e-08	2.6822	0	1.05
15	1.3917	0.5958	71.4071	3.27e-08	2.7024	0	1.08
16	1.8457	0.4481	91.8986	2.88e-06	2.6931	0	1.05
17	2.0000	0.6144	137.0441	8.54e-06	2.6920	0	1.05
18	1.7615	0.8396	128.5384	1.55e-06	2.6975	0	1.01
19	0.5000	0.0010	61.4805	3.03e-22	2.6800	0	0.98
20	1.2316	0.4433	65.0568	3.07e-09	2.6983	0	1.01
21	1.3140	0.0010	63.6885	1.09e-08	2.6800	0	1.06
22	1.7670	0.3641	81.8104	1.55e-06	2.6919	0	1.03
23	1.9988	0.7299	175.8436	8.60e-06	2.6911	0	0.97
24	1.4567	0.2588	67.6954	7.25e-08	2.6902	0	1.05
25	0.7526	0.2893	61.2874	6.71e-15	2.6927	0	1.04
26	0.9282	0.3565	61.7137	3.79e-12	2.6955	0	1.03
27	1.7101	0.8868	126.3171	1.01e-06	2.6988	0	1.06
28	1.8943	0.7141	133.3291	4.23e-06	2.6944	0	1.06
29	0.7823	0.2835	61.3265	2.39e-14	2.6924	0	0.88
30	0.8988	0.0010	61.6467	1.55e-12	2.6800	0	1.02

A.1.2. KC200GT (Polycrystalline)

Table A.8: Optimal parameters for single-diode model of *KC200GT* using BWR.

Run	a	R_s (Ω)	R_p (Ω)	I_0 (A)	I_{pv} (A)	ERR	Time(s)
1	1.0273	0.0010	50.0000	7.13e-10	8.2102	0	1.99
2	0.5000	0.4512	50.0000	1.93e-20	8.2841	0	2.00
3	1.0273	0.0010	50.0000	7.12e-10	8.2102	0	1.97
4	1.0272	0.0010	50.0000	7.12e-10	8.2102	0	2.08
5	1.0273	0.0010	50.0000	7.13e-10	8.2102	0	2.00
6	1.0273	0.0010	50.0000	7.12e-10	8.2102	0	2.11
7	1.0273	0.0010	50.0000	7.13e-10	8.2102	0	2.08
8	0.9850	0.0377	50.0000	2.65e-10	8.2162	0	2.12
9	1.0279	0.0010	50.0203	7.22e-10	8.2102	0	2.02
10	1.0273	0.0010	50.0000	7.14e-10	8.2102	0	2.03
11	0.5000	0.4512	50.0000	1.93e-20	8.2841	0	2.01
12	0.8080	0.1898	50.0000	1.36e-12	8.2412	0	2.06
13	1.0273	0.0010	50.0000	7.13e-10	8.2102	0	2.08
14	1.2592	0.0807	75.6624	5.16e-08	8.2188	0	2.04
15	0.5330	0.4234	50.0000	3.62e-19	8.2795	0	2.07
16	1.0273	0.0010	50.0000	7.13e-10	8.2102	0	2.05
17	0.5000	0.5955	133.4840	2.02e-20	8.2466	0	2.14
18	1.0273	0.0010	50.0000	7.13e-10	8.2102	0	2.01
19	1.0884	0.2342	94.9272	2.72e-09	8.2303	0	2.08
20	1.0273	0.0010	50.0000	7.13e-10	8.2102	0	2.06
21	1.2599	0.2045	172.5042	5.38e-08	8.2197	0	2.04
22	0.5000	0.4512	50.0000	1.93e-20	8.2841	0	2.11
23	1.5396	0.0628	183.9525	1.64e-06	8.2128	0	2.05
24	0.7328	0.2540	50.0000	6.72e-14	8.2517	0	1.97
25	1.2698	0.0010	62.9564	5.96e-08	8.2101	0	1.98
26	1.2310	0.2110	153.9184	3.44e-08	8.2213	0	2.01
27	1.1959	0.0877	68.4800	1.89e-08	8.2205	0	2.04
28	1.0274	0.0010	50.0000	7.14e-10	8.2102	0	1.97
29	1.2627	0.0065	63.0284	5.37e-08	8.2108	0	1.42
30	0.9253	0.0891	50.0000	5.61e-11	8.2246	0	2.01

A.1.3. *Shell SQ85 (Monocrystalline)*

Table A.9: Optimal parameters for single-diode model of *Shell SQ85* using BWR.

Run	a	R_s ()	R_p ()	I_0 (A)	I_{pv} (A)	ERR	Time(s)
1	2.0000	0.0010	117.3684	3.23e-05	5.4500	0	2.10
2	1.5961	0.1279	73.8150	1.52e-06	5.4594	0	2.05
3	2.0000	0.0010	117.3701	3.23e-05	5.4500	0	2.09
4	1.5243	0.0225	50.0000	7.27e-07	5.4524	0	2.00
5	0.6246	0.6689	76.6043	1.06e-16	5.4976	0	2.04
6	1.1757	0.4436	178.8766	7.27e-09	5.4635	0	2.04
7	1.3924	0.3039	112.9848	1.72e-07	5.4647	0	2.08
8	2.0000	0.0010	117.3666	3.23e-05	5.4500	0	1.98
9	1.8364	0.0637	102.2162	1.10e-05	5.4534	0	1.98
10	1.5571	0.0010	50.0000	1.01e-06	5.4501	0	2.00
11	0.8394	0.6035	168.1033	2.04e-12	5.4696	0	2.09
12	0.5000	0.6887	50.0000	7.22e-21	5.5251	0	2.22
13	1.5570	0.0010	50.0000	1.01e-06	5.4501	0	2.08
14	0.8537	0.5355	71.9007	3.20e-12	5.4906	0	2.06
15	0.8259	0.4893	51.9589	1.21e-12	5.5013	0	2.04
16	1.5570	0.0010	50.0000	1.01e-06	5.4501	0	2.09
17	1.5570	0.0010	50.0000	1.01e-06	5.4501	0	2.10
18	1.8117	0.0010	71.9433	9.07e-06	5.4501	0	2.03
19	1.3370	0.3669	182.5335	8.53e-08	5.4610	0	2.06
20	1.9179	0.0042	92.7956	1.91e-05	5.4502	0	2.02
21	0.5000	0.7451	87.4036	7.45e-21	5.4965	0	2.19
22	1.0435	0.3365	50.0000	5.16e-10	5.4867	0	2.20
23	1.8308	0.0785	110.6654	1.06e-05	5.4539	0	2.40
24	2.0000	0.0211	137.5124	3.25e-05	5.4508	0	2.21
25	2.0000	0.0238	140.9149	3.25e-05	5.4509	0	2.06
26	2.0000	0.0010	117.3670	3.23e-05	5.4500	0	2.03
27	1.5570	0.0010	50.0000	1.01e-06	5.4501	0	2.06
28	1.1663	0.3740	77.4148	6.00e-09	5.4763	0	2.15
29	1.1667	0.3505	68.1203	6.00e-09	5.4780	0	2.23
30	1.9908	0.0037	115.7713	3.05e-05	5.4502	0	2.14

A.2. Double-Diode Model

A.2.1. Shell ST40

Table A.10: Optimal parameters for double-diode model of *Shell ST40* using BWR.

Run	a_1	a_2	R_s (Ω)	R_p (Ω)	I_{o1} (A)	I_{o2} (A)	I_{pv} (A)	ERR	Time (s)
1	1.9956	0.5265	0.6914	62.5366	3.76e-07	3.76e-06	2.7336	0	3.53
2	1.9536	1.5450	0.1489	69.1688	3.89e-07	3.89e-06	2.7336	0	0.05
3	1.5043	0.5092	0.0126	63.1526	4.64e-08	4.64e-07	2.7336	0	2.35
4	1.6820	1.1614	0.9215	104.5863	5.79e-07	5.79e-06	2.7336	0	2.18
5	1.7577	0.9141	0.5308	72.4043	6.81e-07	6.81e-06	2.7336	0	3.16
6	1.7121	1.1181	0.8736	84.2778	4.45e-07	4.45e-06	2.7336	0	1.90
7	1.9241	0.9459	0.0391	63.3849	6.08e-07	6.08e-06	2.7336	0	4.40
8	1.7747	1.8985	0.5508	99.1853	8.54e-07	8.54e-06	2.7336	0	1.46
9	1.9771	1.3038	0.9584	80.6245	1.71e-07	1.71e-06	2.7336	0	1.07
10	1.9896	1.4621	0.8529	87.4985	2.80e-07	2.80e-06	2.7336	0	1.44
11	1.8229	1.1684	0.6367	74.5547	7.69e-07	7.69e-06	2.7336	0	1.00
12	1.9866	0.6427	0.4574	61.6760	1.75e-07	1.75e-06	2.7336	0	1.29
13	1.7910	0.7678	0.3149	64.2980	3.57e-07	3.57e-06	2.7336	0	1.68
14	1.9304	1.6488	0.7771	102.4458	4.90e-07	4.90e-06	2.7336	0	1.21
15	1.6972	1.2055	0.1778	64.6116	1.31e-07	1.31e-06	2.7336	0	3.46
16	1.7695	1.3533	0.7995	94.3647	8.64e-07	8.64e-06	2.7336	0	0.79
17	1.5774	0.5816	0.8755	83.5777	2.00e-07	2.00e-06	2.7336	0	0.18
18	1.9574	1.6958	0.7748	108.6473	5.57e-07	5.57e-06	2.7336	0	0.24
19	1.8188	0.6622	0.5871	63.9767	2.83e-07	2.83e-06	2.7336	0	1.12
20	1.7850	1.8416	0.1345	77.4433	9.44e-08	9.44e-07	2.7336	0	0.01
21	1.9736	0.9026	0.5242	65.9171	9.76e-07	9.76e-06	2.7336	0	0.92
22	1.8381	1.5169	0.6902	83.8549	3.41e-07	3.41e-06	2.7336	0	0.89
23	1.9243	1.5037	0.9924	115.9786	7.66e-07	7.66e-06	2.7336	0	3.30
24	1.8292	1.1709	0.0798	64.7616	4.59e-07	4.59e-06	2.7336	0	0.73
25	1.9874	1.1010	0.0094	62.5199	1.62e-07	1.62e-06	2.7336	0	3.28
26	1.7327	1.5974	0.2081	70.9468	1.05e-07	1.05e-06	2.7336	0	1.39
27	1.6326	1.4366	0.5616	76.2561	2.06e-07	2.06e-06	2.7336	0	0.63
28	1.5801	1.2312	0.0831	67.3290	2.27e-07	2.27e-06	2.7336	0	1.23
29	1.3204	1.2444	0.6085	67.1851	6.46e-10	6.46e-09	2.7336	0	3.18
30	1.5631	1.2129	0.2083	69.1281	2.19e-07	2.19e-06	2.7336	0	0.48

A.2.2. *KC200GT (Polycrystalline)*

Table A.11: Optimal parameters for double-diode model of *KC200GT* using BWR.

Run	a_1	a_2	R_s (Ω)	R_p (Ω)	I_{o1} (A)	I_{o2} (A)	I_{pv} (A)	ERR	Time (s)
1	1.6302	0.5677	0.1385	50.5678	4.23e-07	4.23e-06	8.3742	0	0.78
2	1.5745	1.0961	0.0090	57.4192	2.97e-07	2.97e-06	8.3742	0	6.80
3	1.5333	0.5221	0.3162	54.3020	1.35e-07	1.35e-06	8.3742	0	6.64
4	1.4738	0.6009	0.1010	114.8153	6.59e-07	6.59e-06	8.3742	0	3.08
5	1.3586	1.7167	0.0371	187.6331	7.90e-08	7.90e-07	8.3742	0	6.54
6	1.7508	1.1708	0.0681	70.2539	9.68e-07	9.68e-06	8.3742	0	6.80
7	1.9100	1.1359	0.2568	152.2282	2.74e-07	2.74e-06	8.3742	0	4.51
8	1.5720	0.9496	0.0924	74.2269	7.99e-07	7.99e-06	8.3742	0	3.67
9	1.4208	1.4651	0.1060	187.9472	5.28e-08	5.28e-07	8.3742	0	1.08
10	1.6077	0.9916	0.0969	70.8858	8.15e-07	8.15e-06	8.3742	0	7.89
11	1.7436	1.1316	0.1869	101.4884	7.68e-07	7.68e-06	8.3742	0	7.92
12	1.5320	1.4589	0.0051	95.7947	5.17e-07	5.17e-06	8.3742	0	7.36
13	1.9434	1.6451	0.0042	184.4511	8.92e-07	8.92e-06	8.3742	0	1.62
14	1.6487	0.8358	0.0764	55.4456	7.17e-07	7.17e-06	8.3742	0	7.38
15	1.6683	1.3471	0.0647	101.7721	8.33e-07	8.33e-06	8.3742	0	7.40
16	1.9094	1.3432	0.1639	185.5312	2.13e-07	2.13e-06	8.3742	0	2.37
17	1.4956	1.0244	0.3075	145.0292	3.43e-08	3.43e-07	8.3742	0	7.60
18	1.4142	1.3127	0.0025	68.5083	5.04e-08	5.04e-07	8.3742	0	7.11
19	1.6944	0.6433	0.0552	50.8021	8.86e-07	8.86e-06	8.3742	0	4.32
20	1.8734	0.5910	0.4812	75.1333	3.92e-07	3.92e-06	8.3742	0	6.76
21	1.6629	0.8752	0.0621	52.1706	4.80e-07	4.80e-06	8.3742	0	7.29
22	1.5249	1.2572	0.0398	77.0322	3.56e-07	3.56e-06	8.3742	0	1.32
23	1.8773	1.0507	0.2247	80.8807	9.02e-08	9.02e-07	8.3742	0	3.88
24	1.8300	1.0949	0.2214	105.7143	9.23e-07	9.23e-06	8.3742	0	4.05
25	1.5154	1.5672	0.0463	167.5364	2.97e-07	2.97e-06	8.3742	0	2.95
26	1.5328	1.5728	0.0145	134.2437	1.45e-07	1.45e-06	8.3742	0	0.08
27	1.4944	0.8703	0.1907	120.6428	5.02e-07	5.02e-06	8.3742	0	4.05
28	1.9696	0.7026	0.3617	57.9105	2.46e-08	2.46e-07	8.3742	0	4.19
29	1.2784	1.0344	0.2192	74.9367	8.05e-12	8.05e-11	8.3742	0	1.44
30	1.5868	1.3320	0.0987	134.2945	7.88e-07	7.88e-06	8.3742	0	4.07

A.2.3. Shell SQ85

Table A.12: Optimal parameters for double-diode model of *Shell SQ85* using BWR.

Run	a_1	a_2	R_s (Ω)	R_p (Ω)	I_{o1} (A)	I_{o2} (A)	I_{pv} (A)	ERR	Time (s)
1	1.4702	1.3265	0.2492	77.8802	2.01e-07	2.01e-06	5.5590	0	3.43
2	1.5923	1.2912	0.2322	78.4853	6.48e-07	6.48e-06	5.5590	0	3.41
3	1.5701	1.9951	0.1679	129.7135	8.84e-07	8.84e-06	5.5590	0	3.43
4	1.7037	1.7714	0.0520	78.4699	6.19e-07	6.19e-06	5.5590	0	1.91
5	1.9753	1.8530	0.0984	145.2052	4.13e-07	4.13e-06	5.5590	0	3.25
6	1.9016	1.9871	0.0081	116.2622	7.77e-07	7.77e-06	5.5590	0	0.48
7	1.5434	0.8308	0.0783	50.8305	7.14e-07	7.14e-06	5.5590	0	1.05
8	1.7151	1.8363	0.1267	156.6993	9.33e-07	9.33e-06	5.5590	0	2.80
9	1.8636	1.5938	0.0853	65.1387	7.41e-07	7.41e-06	5.5590	0	3.25
10	1.9365	1.5144	0.0453	52.0322	4.20e-07	4.20e-06	5.5590	0	3.20
11	1.8840	1.8432	0.0634	104.7484	4.93e-07	4.93e-06	5.5590	0	0.57
12	1.9669	1.8435	0.1170	168.5214	3.15e-08	3.15e-07	5.5590	0	3.29
13	1.6880	0.7947	0.5416	77.3735	2.16e-07	2.16e-06	5.5590	0	1.23
14	1.6904	1.5145	0.1103	60.7270	2.41e-07	2.41e-06	5.5590	0	3.30
15	1.7391	1.9954	0.0096	119.9133	1.45e-07	1.45e-06	5.5590	0	3.29
16	1.7407	1.4374	0.1574	60.1858	8.40e-08	8.40e-07	5.5590	0	2.50
17	1.4272	1.2789	0.1595	55.7109	1.89e-07	1.89e-06	5.5590	0	3.28
18	1.9927	1.5137	0.1236	63.5184	9.21e-07	9.21e-06	5.5590	0	3.27
19	1.5836	0.5749	0.0667	50.1729	1.00e-06	1.00e-05	5.5590	0	0.90
20	1.6669	1.5469	0.2092	101.2510	1.23e-07	1.23e-06	5.5590	0	3.26
21	1.6084	1.6182	0.0152	54.8399	6.39e-07	6.39e-06	5.5590	0	2.57
22	1.7283	0.7008	0.5536	142.3127	9.55e-07	9.55e-06	5.5590	0	3.25
23	1.8578	1.5521	0.1753	87.6743	8.63e-07	8.63e-06	5.5590	0	3.36
24	1.6534	1.5025	0.0590	52.1421	2.87e-08	2.87e-07	5.5590	0	3.35
25	1.6098	1.5689	0.2293	131.5979	9.58e-08	9.58e-07	5.5590	0	3.26
26	1.9635	1.5014	0.0246	50.0615	9.41e-07	9.41e-06	5.5590	0	1.03
27	1.6010	1.7177	0.0233	62.7697	3.12e-07	3.12e-06	5.5590	0	0.48
28	1.6944	0.8590	0.4659	118.3185	8.64e-07	8.64e-06	5.5590	0	2.51
29	1.6027	1.6992	0.1349	88.8837	7.61e-07	7.61e-06	5.5590	0	0.65
30	1.8666	0.9355	0.5068	106.9141	6.59e-07	6.59e-06	5.5590	0	2.28

B. BMR Algorithm

B.1. Single-Diode Model

B.1.1. Shell ST40 (Thin-Film)

Table B.13: Optimal parameters for single-diode model of *Shell ST40* using BMR.

Run	a	R_s (Ω)	R_p (Ω)	I_0 (A)	I_{pv} (A)	ERR	Time(s)
1	2.0000	0.6344	142.1325	8.56e-06	2.6920	0	1.07
2	1.2207	0.5497	65.8367	2.56e-09	2.7024	0	1.07
3	1.4716	0.4487	71.0834	8.71e-08	2.6969	0	1.12
4	1.0725	0.6588	64.0354	1.48e-10	2.7076	0	1.07
5	1.6959	0.9149	129.1790	8.91e-07	2.6990	0	1.11
6	0.6234	0.0010	61.4853	6.49e-18	2.6800	0	1.09
7	1.7548	1.0000	187.2554	1.50e-06	2.6943	0	1.15
8	1.0594	0.9521	67.1041	1.12e-10	2.7180	0	1.14
9	2.0000	0.5630	126.0796	8.49e-06	2.6920	0	1.09
10	0.5000	0.4831	61.0022	3.05e-22	2.7012	0	1.06
11	1.0613	0.0010	62.0568	1.13e-10	2.6800	0	1.12
12	2.0000	0.3893	102.6604	8.34e-06	2.6902	0	1.10
13	0.5799	1.0000	60.6575	3.18e-19	2.7242	0	1.05
14	0.9899	0.0010	61.8311	2.04e-11	2.6800	0	1.12
15	1.5859	0.0104	67.6532	2.95e-07	2.6804	0	1.09
16	1.3293	0.1175	64.3615	1.37e-08	2.6849	0	1.07
17	1.6373	0.9787	128.9493	5.24e-07	2.7003	0	1.09
18	1.6396	0.2110	71.8825	5.03e-07	2.6879	0	1.09
19	1.5659	1.0000	116.1545	2.58e-07	2.7031	0	1.12
20	1.5992	0.0010	67.8177	3.37e-07	2.6800	0	1.05
21	1.7209	0.0010	70.6279	1.03e-06	2.6800	0	1.09
22	1.4825	0.0010	65.7644	9.70e-08	2.6800	0	1.05
23	0.9516	0.7338	62.7530	7.45e-12	2.7113	0	1.06
24	2.0000	0.4382	107.7652	8.38e-06	2.6909	0	1.09
25	1.8135	0.4195	87.5358	2.25e-06	2.6928	0	1.08
26	1.9840	0.5166	115.4251	7.62e-06	2.6920	0	1.08
27	0.5000	0.0010	61.4825	3.03e-22	2.6800	0	1.06
28	1.5456	0.9301	101.8398	2.07e-07	2.7045	0	1.07
29	0.6483	0.7074	60.9014	3.10e-17	2.7111	0	1.10
30	1.7436	0.0905	72.8448	1.26e-06	2.6833	0	1.10

B.1.2. KC200GT (Polycrystalline)

Table B.14: Optimal parameters for single-diode model of *KC200GT* using BMR.

Run	a	R_s (Ω)	R_p (Ω)	I_0 (A)	I_{pv} (A)	ERR	Time(s)
1	1.2335	0.2097	154.1243	3.59e-08	8.2212	0	2.10
2	0.5000	0.4512	50.0000	1.93e-20	8.2841	0	2.18
3	0.8299	0.1710	50.0000	2.96e-12	8.2381	0	2.12
4	1.3286	0.0308	74.2163	1.38e-07	8.2134	0	2.15
5	0.5899	0.3753	50.0000	2.65e-17	8.2716	0	2.09
6	1.0272	0.0010	50.0000	7.12e-10	8.2102	0	2.30
7	1.0273	0.0010	50.0000	7.13e-10	8.2102	0	2.13
8	1.0273	0.0010	50.0000	7.13e-10	8.2102	0	2.19
9	0.8156	0.1833	50.0000	1.79e-12	8.2401	0	2.11
10	1.0273	0.0010	50.0000	7.13e-10	8.2102	0	2.11
11	1.2140	0.1087	75.5858	2.56e-08	8.2218	0	2.22
12	1.0273	0.0010	50.0000	7.13e-10	8.2102	0	2.10
13	1.0273	0.0010	50.0000	7.13e-10	8.2102	0	2.12
14	1.4639	0.0324	103.3724	7.29e-07	8.2126	0	2.14
15	1.5080	0.0141	107.2939	1.17e-06	8.2111	0	2.20
16	0.8131	0.1854	50.0000	1.64e-12	8.2404	0	2.17
17	1.1749	0.0947	67.2581	1.33e-08	8.2216	0	0.25
18	1.0273	0.0010	50.0000	7.14e-10	8.2102	0	2.14
19	1.5781	0.0303	160.7382	2.38e-06	8.2115	0	2.21
20	1.3139	0.0010	67.0030	1.12e-07	8.2101	0	2.09
21	0.8202	0.1793	50.0000	2.11e-12	8.2394	0	2.19
22	0.5000	0.4512	50.0000	1.93e-20	8.2841	0	2.17
23	1.6711	0.0010	200.0000	5.53e-06	8.2100	0	2.16
24	1.0273	0.0010	50.0000	7.13e-10	8.2102	0	2.21
25	0.5000	0.4512	50.0000	1.93e-20	8.2841	0	2.11
26	0.6895	0.4978	147.6295	9.29e-15	8.2377	0	2.18
27	1.0273	0.0010	50.0000	7.13e-10	8.2102	0	2.15
28	0.6294	0.4180	58.3483	3.35e-16	8.2688	0	2.20
29	1.0273	0.0010	50.0000	7.13e-10	8.2102	0	2.16
30	0.5000	0.4512	50.0000	1.93e-20	8.2841	0	2.09

B.1.3. Shell SQ85 (Monocrystalline)

Table B.15: Optimal parameters for single-diode model of *Shell SQ85* using BMR.

Run	a	R_s (Ω)	R_p (Ω)	I_0 (A)	I_{pv} (A)	ERR	Time(s)
1	1.4689	0.0588	50.0000	4.01e-07	5.4564	0	2.21
2	1.1542	0.4138	100.3448	4.89e-09	5.4725	0	2.35
3	0.5935	0.6425	53.6518	1.39e-17	5.5153	0	2.14
4	1.5322	0.2053	91.9249	8.22e-07	5.4622	0	2.17
5	2.0000	0.0010	117.3588	3.23e-05	5.4500	0	2.27
6	0.8211	0.5962	117.5789	1.07e-12	5.4776	0	2.20
7	1.0590	0.4835	130.8259	7.61e-10	5.4701	0	2.18
8	1.1356	0.3938	78.9634	3.44e-09	5.4772	0	2.14
9	1.0203	0.3601	51.1177	3.07e-10	5.4884	0	2.30
10	1.6575	0.0010	56.2860	2.60e-06	5.4501	0	2.21
11	1.5570	0.0010	50.0000	1.01e-06	5.4501	0	2.16
12	1.5570	0.0010	50.0000	1.01e-06	5.4501	0	2.17
13	2.0000	0.0010	117.3608	3.23e-05	5.4500	0	2.15
14	1.9249	0.0010	93.0542	2.00e-05	5.4501	0	2.21
15	1.3866	0.1126	50.0000	1.52e-07	5.4623	0	2.16
16	1.6135	0.2250	160.5309	1.84e-06	5.4576	0	2.17
17	1.5570	0.0010	50.0000	1.01e-06	5.4501	0	2.15
18	1.5570	0.0010	50.0000	1.01e-06	5.4501	0	2.16
19	1.1650	0.3838	82.1909	5.88e-09	5.4754	0	2.21
20	1.0862	0.4837	167.5087	1.35e-09	5.4657	0	2.19
21	1.5570	0.0010	50.0000	1.01e-06	5.4501	0	2.32
22	1.6318	0.0010	54.4721	2.06e-06	5.4501	0	2.24
23	1.6357	0.0847	68.1981	2.17e-06	5.4568	0	2.19
24	1.9857	0.0010	111.6965	2.96e-05	5.4500	0	2.16
25	1.7333	0.1131	99.6851	5.07e-06	5.4562	0	2.19
26	2.0000	0.0010	117.3644	3.23e-05	5.4500	0	2.13
27	1.5085	0.2817	174.6899	6.56e-07	5.4588	0	2.19
28	1.8213	0.1081	135.7114	1.00e-05	5.4543	0	2.16
29	2.0000	0.0010	117.3648	3.23e-05	5.4500	0	2.16
30	1.5570	0.0010	50.0000	1.01e-06	5.4501	0	2.16

B.2. Double-Diode Model

B.2.1. Shell ST40

Table B.16: Optimal parameters for double-diode model of *Shell ST40* using BMR.

Run	a_1	a_2	R_s (Ω)	R_p (Ω)	I_{o1} (A)	I_{o2} (A)	I_{pv} (A)	ERR	Time (s)
1	1.8058	0.5400	0.0853	61.5221	2.33e-08	2.33e-07	2.7336	0	3.42
2	1.3373	0.5131	0.6560	61.1905	6.43e-10	6.43e-09	2.7336	0	3.41
3	1.5001	0.5690	0.7703	60.8911	9.28e-10	9.28e-09	2.7336	0	3.62
4	1.9850	1.2160	0.1123	64.9245	8.19e-07	8.19e-06	2.7336	0	3.41
5	1.9686	1.9527	0.0147	78.8740	1.29e-07	1.29e-06	2.7336	0	3.55
6	2.0000	1.1818	0.0011	63.2981	3.73e-07	3.73e-06	2.7336	0	3.56
7	1.9009	0.6732	0.0043	62.3127	2.82e-07	2.82e-06	2.7336	0	3.41
8	1.8046	0.6559	0.0012	61.5503	1.27e-08	1.27e-07	2.7336	0	3.39
9	1.7336	0.7306	0.2492	61.2966	1.10e-10	1.10e-09	2.7336	0	3.43
10	1.8438	1.2757	0.4013	69.5939	6.37e-07	6.37e-06	2.7336	0	3.38
11	1.8817	0.7195	0.8286	68.4645	6.67e-07	6.67e-06	2.7336	0	3.43
12	1.6417	0.9601	0.0464	62.7288	7.28e-08	7.28e-07	2.7336	0	3.47
13	1.9109	0.6367	0.5365	61.0902	1.62e-08	1.62e-07	2.7336	0	3.52
14	1.9979	1.8750	0.3619	89.8570	8.07e-07	8.07e-06	2.7336	0	3.49
15	1.9451	1.0114	0.2289	62.9991	3.21e-07	3.21e-06	2.7336	0	3.46
16	1.8983	0.5168	0.9749	65.1987	3.94e-07	3.94e-06	2.7336	0	3.35
17	1.8494	0.8759	0.4822	68.3785	8.46e-07	8.46e-06	2.7336	0	3.38
18	1.9990	0.5004	0.1796	62.0005	3.03e-07	3.03e-06	2.7336	0	3.43
19	1.0596	0.5743	0.6046	61.0786	7.86e-12	7.86e-11	2.7336	0	3.44
20	1.9981	0.7187	0.2286	63.5699	8.99e-07	8.99e-06	2.7336	0	3.40
21	1.9104	0.9900	0.2515	62.4151	1.32e-07	1.32e-06	2.7336	0	3.43
22	1.9982	0.5806	0.5260	61.7996	2.28e-07	2.28e-06	2.7336	0	3.46
23	1.8468	1.1143	0.0249	62.6831	1.01e-07	1.01e-06	2.7336	0	3.39
24	1.8770	0.6487	0.0039	61.9505	1.42e-07	1.42e-06	2.7336	0	3.53
25	1.8873	1.7321	0.9991	197.3223	9.92e-07	9.92e-06	2.7336	0	3.31
26	1.7121	0.8316	0.0300	61.5462	1.90e-10	1.90e-09	2.7336	0	3.40
27	1.9898	0.5160	0.3087	61.2051	1.05e-08	1.05e-07	2.7336	0	3.40
28	1.9476	1.8044	0.0016	73.0430	4.23e-09	4.23e-08	2.7336	0	3.46
29	1.9144	0.5180	0.1926	63.6196	6.45e-07	6.45e-06	2.7336	0	3.41
30	1.9057	1.4162	0.9028	86.6527	1.66e-07	1.66e-06	2.7336	0	3.38

B.2.2. *KC200GT (Polycrystalline)*

Table B.17: Optimal parameters for double-diode model of *KC200GT* using BMR.

Run	a_1	a_2	R_s (Ω)	R_p (Ω)	I_{o1} (A)	I_{o2} (A)	I_{pv} (A)	ERR	Time (s)
1	1.0442	0.7540	0.0024	50.0166	9.41e-10	9.41e-09	8.3742	0	3.58
2	1.5324	0.5411	0.0022	50.1624	3.15e-07	3.15e-06	8.3742	0	3.56
3	1.2637	0.7330	0.3648	64.4453	1.18e-09	1.18e-08	8.3742	0	3.56
4	1.3547	0.5653	0.3753	50.8742	4.51e-09	4.51e-08	8.3742	0	3.78
5	1.6971	0.7447	0.0865	50.2869	5.99e-07	5.99e-06	8.3742	0	3.63
6	1.4099	0.8363	0.0015	53.9622	1.39e-07	1.39e-06	8.3742	0	3.70
7	1.6879	0.7222	0.0089	50.8575	9.48e-07	9.48e-06	8.3742	0	3.61
8	1.6767	0.5001	0.0212	50.0274	8.49e-07	8.49e-06	8.3742	0	3.68
9	1.1478	1.2168	0.1624	95.2183	5.38e-10	5.38e-09	8.3742	0	3.59
10	1.5935	0.8158	0.0013	52.7692	5.71e-07	5.71e-06	8.3742	0	3.55
11	1.5624	0.5202	0.0020	50.0099	3.93e-07	3.93e-06	8.3742	0	3.69
12	1.4106	1.0002	0.1350	189.8023	3.97e-07	3.97e-06	8.3742	0	3.66
13	1.9617	0.9775	0.0565	50.9805	2.86e-07	2.86e-06	8.3742	0	3.72
14	1.6817	1.1436	0.2558	192.5735	3.24e-07	3.24e-06	8.3742	0	3.58
15	1.7331	1.0090	0.2869	112.0015	2.77e-07	2.77e-06	8.3742	0	3.58
16	1.8675	1.0924	0.1423	71.0451	8.98e-07	8.98e-06	8.3742	0	3.57
17	1.3034	0.7743	0.0213	55.3038	5.11e-08	5.11e-07	8.3742	0	3.66
18	1.8175	0.9292	0.0417	50.2220	5.46e-07	5.46e-06	8.3742	0	3.69
19	1.8239	0.8099	0.0858	50.0437	9.36e-07	9.36e-06	8.3742	0	3.63
20	1.8817	1.0208	0.0013	50.3330	2.60e-07	2.60e-06	8.3742	0	3.68
21	1.5080	1.3947	0.0058	96.3903	9.30e-07	9.30e-06	8.3742	0	3.61
22	1.3791	1.5716	0.0232	115.2074	8.60e-08	8.60e-07	8.3742	0	3.70
23	1.6937	0.5334	0.0347	50.2006	9.27e-07	9.27e-06	8.3742	0	3.72
24	1.8250	1.0250	0.0014	50.0239	2.96e-08	2.96e-07	8.3742	0	3.62
25	1.6332	1.1632	0.0766	72.8047	5.65e-07	5.65e-06	8.3742	0	3.62
26	1.5927	1.4287	0.0388	105.7836	4.94e-07	4.94e-06	8.3742	0	3.60
27	1.3895	1.7823	0.0140	80.8836	2.96e-07	2.96e-06	8.3742	0	3.66
28	1.6611	1.0456	0.0071	59.3309	9.69e-07	9.69e-06	8.3742	0	3.70
29	1.8807	0.5413	0.5266	87.4063	5.25e-07	5.25e-06	8.3742	0	3.72
30	1.4941	0.7963	0.0036	50.2907	1.87e-07	1.87e-06	8.3742	0	3.55

B.2.3. *Shell SQ85*

Table B.18: Optimal parameters for double-diode model of *Shell SQ85* using BMR.

Run	a_1	a_2	R_s (Ω)	R_p (Ω)	I_{o1} (A)	I_{o2} (A)	I_{pv} (A)	ERR	Time (s)
1	1.9814	1.9727	0.0105	113.9955	3.70e-07	3.70e-06	5.5590	0	3.50
2	1.9408	1.9999	0.0019	116.9629	9.81e-07	9.81e-06	5.5590	0	3.46
3	1.2354	0.7562	0.5196	50.1373	1.95e-10	1.95e-09	5.5590	0	3.49
4	1.5205	0.5061	0.1951	63.4326	5.65e-07	5.65e-06	5.5590	0	3.53
5	1.7931	1.8558	0.0153	82.7090	5.89e-07	5.89e-06	5.5590	0	3.41
6	1.5208	1.7861	0.0033	50.2814	6.10e-07	6.10e-06	5.5590	0	3.42
7	1.4919	1.9592	0.0642	66.1392	3.59e-07	3.59e-06	5.5590	0	3.40
8	1.6568	1.4611	0.1615	64.0911	1.09e-07	1.09e-06	5.5590	0	3.40
9	1.6396	1.3746	0.2843	94.0951	1.11e-07	1.11e-06	5.5590	0	3.43
10	1.8194	0.8179	0.4848	50.4412	1.05e-08	1.05e-07	5.5590	0	3.37
11	1.6070	1.7884	0.0023	61.0064	7.19e-07	7.19e-06	5.5590	0	3.41
12	1.3648	1.6856	0.0134	59.4834	3.63e-09	3.63e-08	5.5590	0	3.44
13	1.7450	1.4752	0.0555	50.1234	1.59e-08	1.59e-07	5.5590	0	3.61
14	1.5515	0.5551	0.6996	128.4673	6.71e-08	6.71e-07	5.5590	0	3.37
15	1.9181	1.5487	0.0082	50.1358	1.30e-09	1.30e-08	5.5590	0	3.36
16	1.5561	0.5003	0.0216	50.8919	9.72e-07	9.72e-06	5.5590	0	3.42
17	1.6984	1.9879	0.0011	93.3368	8.57e-07	8.57e-06	5.5590	0	3.45
18	1.6286	0.5351	0.7525	199.0567	8.69e-09	8.69e-08	5.5590	0	3.48
19	1.7609	1.5185	0.0301	51.0622	2.95e-07	2.95e-06	5.5590	0	3.39
20	1.8198	1.5543	0.0091	50.9701	2.59e-07	2.59e-06	5.5590	0	3.52
21	1.7426	0.5787	0.5143	64.9985	9.37e-07	9.37e-06	5.5590	0	3.44
22	1.6035	1.7609	0.0552	65.6268	9.88e-07	9.88e-06	5.5590	0	3.38
23	1.6979	0.5577	0.6590	199.7395	5.66e-07	5.66e-06	5.5590	0	3.45
24	1.7630	1.8605	0.0011	78.3176	4.79e-07	4.79e-06	5.5590	0	3.52
25	1.6456	0.8651	0.2407	50.1496	7.34e-07	7.34e-06	5.5590	0	3.36
26	1.7886	1.5626	0.0018	50.4282	3.34e-08	3.34e-07	5.5590	0	3.44
27	1.6893	1.4621	0.0619	51.6681	4.15e-07	4.15e-06	5.5590	0	3.42
28	1.6585	0.8123	0.4781	53.5873	1.07e-07	1.07e-06	5.5590	0	3.37
29	1.3981	1.9936	0.0219	90.7298	4.13e-08	4.13e-07	5.5590	0	3.43
30	1.9967	1.9727	0.0184	120.5958	3.15e-07	3.15e-06	5.5590	0	3.48

C. JAYA Algorithm

C.1. Single-Diode Model

C.1.1. Shell ST40 (Thin-Film)

Table C.19: Optimal parameters for single-diode model of *Shell ST40* using JAYA.

Run	a	R_s (Ω)	R_p (Ω)	I_0 (A)	I_{pv} (A)	ERR	Time(s)
1	2.0000	0.3740	101.2313	8.33e-06	2.6899	0	1.46
2	1.0825	0.0010	62.1405	1.80e-10	2.6800	0	0.14
3	0.6895	0.7133	60.9815	3.16e-16	2.7113	0	1.53
4	1.0259	0.9791	66.5231	5.13e-11	2.7194	0	0.79
5	0.5187	0.2947	61.1888	1.86e-21	2.6929	0	0.38
6	1.3434	0.0010	63.9836	1.66e-08	2.6800	0	3.14
7	2.0000	0.7718	200.0000	8.72e-06	2.6904	0	0.47
8	0.5000	0.1188	61.3632	3.03e-22	2.6852	0	1.87
9	2.0000	0.0010	80.5768	8.10e-06	2.6800	0	0.35
10	2.0000	0.0010	80.5767	8.10e-06	2.6800	0	0.48
11	2.0000	0.5319	120.6052	8.46e-06	2.6918	0	3.91
12	1.8328	0.4822	93.1398	2.62e-06	2.6939	0	3.84
13	0.5630	0.3900	61.0997	8.56e-20	2.6971	0	0.15
14	0.7340	0.4268	61.1783	2.88e-15	2.6987	0	0.32
15	1.4660	0.0010	65.5177	8.01e-08	2.6800	0	0.58
16	0.5000	1.0000	60.5306	3.08e-22	2.7243	0	0.14
17	0.7306	0.0010	61.5065	2.44e-15	2.6800	0	0.51
18	1.9670	0.7209	158.2633	6.98e-06	2.6922	0	1.57
19	1.8610	0.0010	74.9031	3.13e-06	2.6800	0	2.42
20	1.7730	1.0000	200.0000	1.74e-06	2.6934	0	1.36
21	0.5959	0.0010	61.4833	1.00e-18	2.6800	0	0.23
22	0.5000	0.3838	61.0997	3.05e-22	2.6968	0	1.65
23	1.6184	1.0000	129.0635	4.38e-07	2.7008	0	1.48
24	1.7677	1.0000	196.1318	1.67e-06	2.6937	0	0.45
25	0.6312	0.7999	60.8296	1.08e-17	2.7152	0	0.10
26	1.6288	0.9391	118.2015	4.81e-07	2.7013	0	3.98
27	0.5000	0.9505	60.5689	3.08e-22	2.7221	0	0.08
28	1.5517	0.7643	87.4583	2.17e-07	2.7034	0	2.71
29	1.4889	0.6435	77.1432	1.08e-07	2.7024	0	2.52
30	2.0000	0.5645	126.3554	8.49e-06	2.6920	0	3.93

C.1.2. KC200GT (Polycrystalline)

Table C.20: Optimal parameters for single-diode model of *KC200GT* using JAYA.

Run	a	R_s (Ω)	R_p (Ω)	I_0 (A)	I_{pv} (A)	ERR	Time(s)
1	1.4382	0.0010	84.1046	5.40e-07	8.2101	0	0.79
2	1.5794	0.0010	126.7525	2.40e-06	8.2101	0	0.77
3	1.2164	0.1346	83.9885	2.68e-08	8.2232	0	0.76
4	0.5000	0.5392	67.0968	1.97e-20	8.2760	0	0.77
5	1.0273	0.0010	50.0000	7.13e-10	8.2102	0	0.80
6	1.6337	0.0010	161.0948	3.98e-06	8.2101	0	0.81
7	1.6589	0.0073	200.0000	4.98e-06	8.2103	0	0.87
8	1.5897	0.0010	131.9580	2.65e-06	8.2101	0	0.73
9	1.0273	0.0010	50.0000	7.13e-10	8.2102	0	0.79
10	1.6614	0.0020	190.3854	5.09e-06	8.2101	0	0.79
11	1.6711	0.0010	200.0000	5.53e-06	8.2100	0	0.75
12	1.3947	0.0010	76.8853	3.21e-07	8.2101	0	0.79
13	1.2877	0.0235	67.8226	7.77e-08	8.2128	0	0.76
14	0.5000	0.6069	190.1731	2.04e-20	8.2362	0	0.75
15	1.3580	0.0010	71.9271	2.02e-07	8.2101	0	0.81
16	1.6712	0.0010	200.0000	5.53e-06	8.2100	0	0.87
17	1.6711	0.0010	200.0000	5.53e-06	8.2100	0	0.81
18	1.0273	0.0010	50.0000	7.13e-10	8.2102	0	0.40
19	1.0273	0.0010	50.0000	7.13e-10	8.2102	0	0.54
20	1.6676	0.0010	195.5287	5.37e-06	8.2100	0	0.80
21	1.5817	0.0046	131.2384	2.45e-06	8.2103	0	0.76
22	1.6381	0.0010	164.8169	4.14e-06	8.2100	0	0.81
23	1.0273	0.0010	50.0000	7.13e-10	8.2102	0	0.70
24	1.6712	0.0010	200.0000	5.53e-06	8.2100	0	0.76
25	1.6443	0.0145	199.0203	4.39e-06	8.2106	0	0.75
26	0.5792	0.3844	50.0000	1.26e-17	8.2731	0	0.78
27	1.0273	0.0010	50.0000	7.13e-10	8.2102	0	0.77
28	1.0273	0.0010	50.0000	7.13e-10	8.2102	0	0.78
29	0.5000	0.5952	132.5964	2.02e-20	8.2469	0	0.76
30	1.6207	0.0019	152.4129	3.54e-06	8.2101	0	0.74

C.1.3. Shell SQ85 (Monocrystalline)

Table C.21: Optimal parameters for single-diode model of *Shell SQ85* using JAYA.

Run	a	R_s (Ω)	R_p (Ω)	I_0 (A)	I_{pv} (A)	ERR	Time(s)
1	1.5570	0.0010	50.0000	1.01e-06	5.4501	0	0.86
2	2.0000	0.0500	187.6771	3.27e-05	5.4515	0	0.80
3	1.5570	0.0010	50.0000	1.01e-06	5.4501	0	0.77
4	2.0000	0.0010	117.3640	3.23e-05	5.4500	0	0.19
5	2.0000	0.0546	200.0000	3.28e-05	5.4515	0	0.80
6	2.0000	0.0546	200.0000	3.28e-05	5.4515	0	0.74
7	2.0000	0.0010	117.3639	3.23e-05	5.4500	0	0.74
8	2.0000	0.0402	166.4875	3.26e-05	5.4513	0	1.09
9	1.8063	0.1295	157.2574	9.01e-06	5.4545	0	0.14
10	2.0000	0.0010	117.3639	3.23e-05	5.4500	0	0.21
11	1.0856	0.4248	81.1396	1.30e-09	5.4785	0	1.03
12	0.7109	0.6633	155.8383	1.16e-14	5.4732	0	1.05
13	2.0000	0.0010	117.3634	3.23e-05	5.4500	0	1.15
14	1.8554	0.1203	190.0807	1.29e-05	5.4535	0	1.10
15	2.0000	0.0010	117.3712	3.23e-05	5.4500	0	1.18
16	1.7302	0.0010	62.4694	4.81e-06	5.4501	0	1.22
17	2.0000	0.0046	120.4674	3.23e-05	5.4502	0	1.02
18	1.7410	0.1763	193.3915	5.50e-06	5.4550	0	1.11
19	0.5000	0.7394	79.4271	7.42e-21	5.5007	0	1.05
20	1.0868	0.3585	57.9162	1.31e-09	5.4837	0	1.04
21	2.0000	0.0091	124.6253	3.24e-05	5.4504	0	1.06
22	2.0000	0.0010	117.3639	3.23e-05	5.4500	0	0.12
23	1.0795	0.4920	187.9381	1.18e-09	5.4643	0	1.02
24	0.5312	0.6724	51.0140	1.21e-19	5.5218	0	1.07
25	1.2927	0.1740	50.0000	4.34e-08	5.4690	0	1.09
26	2.0000	0.0010	117.3641	3.23e-05	5.4500	0	1.06
27	2.0000	0.0010	117.3546	3.23e-05	5.4500	0	1.11
28	1.5749	0.1055	65.1131	1.23e-06	5.4588	0	0.98
29	2.0000	0.0010	117.3643	3.23e-05	5.4500	0	1.01
30	1.6715	0.0010	57.3550	2.94e-06	5.4501	0	0.82

C.2. Double-Diode Model

C.2.1. Shell ST40

Table C.22: Optimal parameters for double-diode model of *Shell ST40* using JAYA.

Run	a_1	a_2	R_s (Ω)	R_p (Ω)	I_{o1} (A)	I_{o2} (A)	I_{pv} (A)	ERR	Time (s)
1	1.7440	1.8783	0.8878	192.7373	4.67e-08	4.67e-07	2.7336	0	1.12
2	1.9932	1.9729	0.7742	185.7348	5.95e-07	5.95e-06	2.7336	0	0.40
3	1.9908	1.9623	0.7916	189.6419	4.60e-07	4.60e-06	2.7336	0	0.04
4	1.8832	0.6087	0.1371	61.4190	1.80e-08	1.80e-07	2.7336	0	0.17
5	1.8161	1.1433	0.9510	89.2623	8.14e-07	8.14e-06	2.7336	0	0.07
6	1.7756	0.8101	0.1824	65.6819	5.51e-07	5.51e-06	2.7336	0	0.03
7	1.9986	1.8212	0.9297	199.3614	9.94e-07	9.94e-06	2.7336	0	0.05
8	1.8902	1.6185	0.8935	119.1948	7.83e-07	7.83e-06	2.7336	0	0.12
9	1.8154	1.7569	0.3477	80.5871	6.15e-09	6.15e-08	2.7336	0	0.08
10	1.9891	0.7381	0.7366	63.8953	5.39e-07	5.39e-06	2.7336	0	0.10
11	1.9306	0.9542	0.5915	62.3667	2.07e-08	2.07e-07	2.7336	0	0.07
12	1.9835	1.9913	0.1232	84.7141	7.75e-08	7.75e-07	2.7336	0	0.03
13	1.9945	0.5298	0.9340	66.2826	8.44e-07	8.44e-06	2.7336	0	0.14
14	1.9902	0.9622	0.3596	63.1268	4.13e-07	4.13e-06	2.7336	0	0.23
15	1.9968	1.7877	0.9727	197.0536	3.35e-07	3.35e-06	2.7336	0	0.12
16	1.6823	1.5775	0.8496	98.2475	5.85e-08	5.85e-07	2.7336	0	0.05
17	1.9724	1.9896	0.1134	84.2081	3.80e-08	3.80e-07	2.7336	0	0.02
18	1.9416	0.6161	0.6517	63.8182	4.99e-07	4.99e-06	2.7336	0	0.03
19	1.9491	0.5253	0.1118	63.9703	9.48e-07	9.48e-06	2.7336	0	0.22
20	1.9987	0.7428	0.3273	63.9123	9.27e-07	9.27e-06	2.7336	0	0.06
21	1.9710	0.7699	0.1203	62.2100	3.23e-07	3.23e-06	2.7336	0	0.04
22	1.9697	1.4757	0.0676	66.9361	4.12e-07	4.12e-06	2.7336	0	0.69
23	1.8881	1.9741	0.5496	117.6460	2.87e-07	2.87e-06	2.7336	0	0.22
24	1.7908	1.9043	0.0241	75.9246	5.12e-07	5.12e-06	2.7336	0	0.04
25	1.9288	1.9906	0.0015	80.1476	1.10e-08	1.10e-07	2.7336	0	0.07
26	1.9914	0.5670	0.9990	60.8540	3.27e-08	3.27e-07	2.7336	0	0.09
27	1.9951	1.9868	0.7679	189.6890	6.30e-07	6.30e-06	2.7336	0	0.16
28	1.8174	1.9972	0.0612	79.0908	9.47e-07	9.47e-06	2.7336	0	0.22
29	1.9698	1.8235	0.0077	73.7891	2.49e-08	2.49e-07	2.7336	0	0.11
30	1.9999	1.4766	0.1494	66.9429	1.51e-08	1.51e-07	2.7336	0	0.03

C.2.2. KC200GT (Polycrystalline)

Table C.23: Optimal parameters for double-diode model of *KC200GT* using JAYA.

Run	a_1	a_2	R_s (Ω)	R_p (Ω)	I_{o1} (A)	I_{o2} (A)	I_{pv} (A)	ERR	Time (s)
1	1.8418	0.5048	0.3660	50.0750	5.39e-07	5.39e-06	8.3742	0	0.42
2	1.8043	1.0700	0.0078	51.8204	3.12e-09	3.12e-08	8.3742	0	0.20
3	1.0911	0.5008	0.0510	50.0146	1.64e-09	1.64e-08	8.3742	0	1.37
4	1.9400	0.5029	0.3625	50.0478	9.98e-07	9.98e-06	8.3742	0	0.35
5	1.9760	1.0208	0.0101	50.7432	4.64e-07	4.64e-06	8.3742	0	0.08
6	1.7234	1.2739	0.2040	191.4914	1.05e-08	1.05e-07	8.3742	0	0.14
7	1.9984	1.6438	0.0085	190.2121	7.71e-07	7.71e-06	8.3742	0	0.17
8	1.7783	0.9886	0.0576	53.7316	5.92e-07	5.92e-06	8.3742	0	0.06
9	1.5559	1.3872	0.0397	112.9375	9.96e-07	9.96e-06	8.3742	0	0.34
10	1.9904	0.5543	0.3498	50.1999	9.94e-07	9.94e-06	8.3742	0	0.05
11	1.6449	1.4619	0.0644	147.2554	8.03e-07	8.03e-06	8.3742	0	1.40
12	1.3909	0.5443	0.0527	51.4128	8.58e-08	8.58e-07	8.3742	0	0.09
13	1.7225	1.2345	0.0033	66.6914	9.81e-07	9.81e-06	8.3742	0	0.32
14	1.7267	1.5955	0.0062	143.0492	2.32e-07	2.32e-06	8.3742	0	0.23
15	1.9765	1.0822	0.0111	52.8324	2.56e-07	2.56e-06	8.3742	0	0.45
16	1.9532	1.4422	0.0047	88.9666	9.97e-07	9.97e-06	8.3742	0	0.71
17	1.7814	0.5046	0.3305	52.8990	7.39e-07	7.39e-06	8.3742	0	1.06
18	1.9935	0.6489	0.3307	52.9284	7.82e-07	7.82e-06	8.3742	0	0.27
19	1.9398	1.6521	0.0016	179.3202	2.47e-08	2.47e-07	8.3742	0	0.05
20	1.8638	1.6112	0.0258	188.6960	2.87e-07	2.87e-06	8.3742	0	0.57
21	1.9792	0.5113	0.3814	50.3437	1.00e-06	1.00e-05	8.3742	0	1.06
22	1.9994	1.6047	0.0262	186.5962	9.57e-07	9.57e-06	8.3742	0	0.80
23	1.4995	0.9442	0.0444	50.7749	6.31e-08	6.31e-07	8.3742	0	0.45
24	1.9154	0.8177	0.4193	172.6346	9.39e-07	9.39e-06	8.3742	0	0.94
25	1.8270	0.8165	0.1394	51.4599	7.35e-07	7.35e-06	8.3742	0	1.01
26	1.5583	1.1831	0.2039	120.7961	7.91e-08	7.91e-07	8.3742	0	1.20
27	1.9948	1.0057	0.0019	50.5333	9.98e-07	9.98e-06	8.3742	0	0.12
28	1.9806	1.1364	0.0027	54.5812	8.25e-08	8.25e-07	8.3742	0	0.03
29	1.9329	1.6644	0.0015	196.9617	4.59e-07	4.59e-06	8.3742	0	0.61
30	1.9035	1.0206	0.0337	51.6922	2.81e-07	2.81e-06	8.3742	0	0.16

C.2.3. Shell SQ85

Table C.24: Optimal parameters for double-diode model of *Shell SQ85* using JAYA.

Run	a_1	a_2	R_s (Ω)	R_p (Ω)	I_{o1} (A)	I_{o2} (A)	I_{pv} (A)	ERR	Time (s)
1	1.9946	1.2450	0.2895	67.8140	9.62e-07	9.62e-06	5.5590	0	0.25
2	1.9774	1.9837	0.0057	114.5062	1.19e-07	1.19e-06	5.5590	0	0.08
3	1.5428	1.6728	0.0062	52.0881	5.97e-07	5.97e-06	5.5590	0	0.14
4	1.9961	1.9521	0.0202	113.5314	4.45e-07	4.45e-06	5.5590	0	0.06
5	1.9356	0.9891	0.5261	152.4359	1.77e-08	1.77e-07	5.5590	0	0.04
6	1.9351	1.9967	0.0436	169.6066	1.58e-07	1.58e-06	5.5590	0	0.47
7	1.9802	1.9969	0.0083	122.2422	5.78e-07	5.78e-06	5.5590	0	0.20
8	1.9973	1.3935	0.0999	50.6567	9.66e-07	9.66e-06	5.5590	0	0.21
9	1.9901	1.9654	0.0078	109.2567	2.46e-07	2.46e-06	5.5590	0	0.13
10	1.9418	0.8608	0.5675	103.5260	9.48e-09	9.48e-08	5.5590	0	0.92
11	1.9895	1.3585	0.1649	55.7698	9.98e-07	9.98e-06	5.5590	0	0.31
12	1.9895	1.9984	0.0029	118.1495	9.13e-07	9.13e-06	5.5590	0	0.02
13	1.9860	1.9693	0.0267	126.9792	5.52e-07	5.52e-06	5.5590	0	0.11
14	1.8366	1.6321	0.1992	139.2122	5.42e-07	5.42e-06	5.5590	0	0.29
15	1.9602	1.4691	0.2251	84.6293	5.79e-09	5.79e-08	5.5590	0	0.15
16	1.6850	1.2087	0.3741	196.1184	8.34e-07	8.34e-06	5.5590	0	0.22
17	1.9143	1.4414	0.3001	162.2359	7.43e-07	7.43e-06	5.5590	0	1.66
18	1.9984	1.9807	0.0086	115.8263	8.41e-07	8.41e-06	5.5590	0	0.60
19	1.6796	1.6695	0.0111	58.6435	3.92e-07	3.92e-06	5.5590	0	0.11
20	1.6580	0.5242	0.6950	198.4982	3.22e-07	3.22e-06	5.5590	0	0.40
21	1.9625	1.9985	0.0013	116.9369	4.60e-08	4.60e-07	5.5590	0	0.35
22	1.9964	1.6937	0.0791	76.1287	4.24e-07	4.24e-06	5.5590	0	0.06
23	1.9998	1.9425	0.0809	199.0605	9.95e-07	9.95e-06	5.5590	0	0.22
24	1.8956	1.8775	0.1095	190.4242	5.61e-07	5.61e-06	5.5590	0	0.34
25	1.8919	1.7791	0.0313	75.9220	6.23e-07	6.23e-06	5.5590	0	0.15
26	1.9529	1.4395	0.0657	50.3393	9.34e-07	9.34e-06	5.5590	0	0.16
27	1.9888	0.5009	0.6644	51.0699	6.70e-07	6.70e-06	5.5590	0	0.07
28	1.5650	1.4428	0.0035	50.0968	9.99e-07	9.99e-06	5.5590	0	0.52
29	1.9515	1.9982	0.0225	137.8560	2.62e-07	2.62e-06	5.5590	0	0.39
30	1.6469	1.8516	0.0738	99.2042	5.47e-07	5.47e-06	5.5590	0	0.14